STRUCTURAL BIOLOGY

Structural basis for CEP192-mediated regulation of centrosomal AURKA

Jin-Gyeong Park[1,2], Hanul Jeon[1], Sangchul Shin[3], Chiman Song[1,4], Hyomin Lee[4,5], Nak-Kyoon Kim[6], Eunice EunKyeong Kim[1], Kwang Yeon Hwang[2], Bong-Jin Lee[7], In-Gyun Lee[1,4]*

Aurora kinase A (AURKA) performs critical functions in mitosis. Thus, the activity and subcellular localization of AURKA are tightly regulated and depend on diverse factors including interactions with the multiple binding cofactors. How these different cofactors regulate AURKA to elicit different levels of activity at distinct subcellular locations and times is poorly understood. Here, we identified a conserved region of CEP192, the major cofactor of AURKA, that mediates the interaction with AURKA. Quantitative binding studies were performed to map the interactions of a conserved helix (Helix-1) within CEP192. The crystal structure of Helix-1 bound to AURKA revealed a distinct binding site that is different from other cofactor proteins such as TPX2. Inhibiting the interaction between Helix-1 and AURKA in cells led to the mitotic defects, demonstrating the importance of the interaction. Collectively, we revealed a structural basis for the CEP192-mediated AURKA regulation at the centrosome, which is distinct from TPX2-mediated regulation on the spindle microtubule.

INTRODUCTION

Aurora kinase A (AURKA) is a serine/threonine kinase that performs critical functions, especially during mitosis, including centrosome maturation, centrosome separation, and bipolar spindle formation (*1*). Given its key roles in mitosis, the spatiotemporal activity of AURKA is tightly regulated by the numerous intramolecular and intermolecular factors and by association with numerous cofactor proteins to ensure that a complete set of chromosomes are properly segregated into two daughter cells (*2*–*4*). These cofactor proteins all work together to regulate the activity, localization, and function of AURKA in each distinct biological context to accomplish a diverse repertoire of biological responses (*5*–*8*). Among these diverse interacting cofactor proteins, centrosomal protein of 192 kDa (CEP192) and targeting protein for Xklp2 (TPX2) have been regarded as two major cofactors (*3*), as they orchestrate AURKA activity in two distinct mitotic spindle assembly pathways (centrosome-mediated and chromatin-mediated, respectively) (*3*, *9*). On the basis of structural, biophysical, and cellular approaches, we shed light on the structural basis for the CEP192-mediated regulation of the centrosomal AURKA activity.

The following spatially distinct pools of AURKA are present within the cells: pools at the centrosomes and on the spindle microtubules (MTs) (*2*, *10*). Two pools of AURKA are recruited either to spindle MTs by TPX2 or to centrosomes by CEP192 (*6*, *7*, *11*). The roles of AURKA in chromatin-mediated spindle MT formation and assembly closely depend on the interaction of AURKA with TPX2, the first cofactor discovered and has been extensively studied, making it one of the best characterized cofactors. During M phase, TPX2 directs AURKA toward spindle MTs, at which TPX2 activates AURKA to promote the MT nucleation; this occurs through mechanisms that are relatively well understood in terms of molecular and structural underpinnings (*12*). A series of biophysical and molecular dynamics studies combined with TPX2-AURKA complex crystal structures revealed the detailed molecular basis of how TPX2 binding activates AURKA both in vitro and in cells at spindle MT (*13*–*15*). The very N-terminal region of TPX2 (residues 1 to 43) constitutes a minimal and essential AURKA binding site, and the binding allosterically activates AURKA. Key structural changes in AURKA induced by TPX2 binding include (i) a shift of the "DFG motif" to the active "DFG-in" conformation and (ii) stabilization of the interaction network around the active site and the rotation of the αC helix. These structural changes can allosterically activate the spindle pool of AURKA, which is maintained in the unphosphorylated state through the action of the protein phosphatase PP6 (*16*–*19*).

In contrast to the spindle MT-associated pool of AURKA that is activated by TPX2, the centrosomal pool of AURKA is activated through autophosphorylation at its activation loop, which is mediated by the interaction with CEP192 as well as other centrosomal cofactors such as Ajuba, NEDD9, and nucleophosmin (*6*–*8*, *20*, *21*). CEP192 binding promotes the oligomerization of AURKA, thus increasing the local concentration of AURKA at the centrosome to promote the autophosphorylation of the kinase. Unlike TPX2, CEP192 seems to act as a scaffold rather than a direct activator, as CEP192 binding itself does not activate the kinase (*6*, *7*). This observation raises the question of how the differential binding of different cofactor induces specific conformational transitions and regulates AURKA activity.

Here, we show that a conserved helix (Helix-1) and its flanking regions (CEP192 residues 506 to 530) within the AURKA-binding domain (AURKA-BD) of CEP192 interact with AURKA. The interactions were quantitatively characterized using isothermal titration calorimetry (ITC) and fluorescence polarization (FP). In contrast to the binding of TPX2, which robustly activates AURKA, the binding

[1]Biomedical Research Division, Korea Institute of Science and Technology, Seoul 02792, South Korea. [2]Department of Biotechnology, College of Life Sciences and Biotechnology, Korea University, Seoul 02841, South Korea. [3]Technology Support Center, Korea Institute of Science and Technology, Seoul 02792, South Korea. [4]Department of Biological Chemistry, University of Science and Technology, Daejeon 34113, South Korea. [5]Chemical Kinomics Research Center, Korea Institute of Science and Technology, Seoul 02792, South Korea. [6]Advanced Analysis Center, Korea Institute of Science and Technology, Seoul 02792, South Korea. [7]The Research Institute of Pharmaceutical Sciences, College of Pharmacy, Seoul National University, Seoul 08826, South Korea.
*Corresponding author. Email: ik86@kist.re.kr

of CEP192 was insufficient to activate AURKA. We report a crystal structure of the essential AURKA binding segment of CEP192 in complex with AURKA, revealing that CEP192 binds to a distinct region on AURKA compared to the TPX2 binding site. The binding elicits different structural outputs, potentially explaining why the CEP192 binding by itself cannot activate the kinase. Supporting the importance of the interaction, overexpression of the CEP192 Helix-1 in cells perturbs the interaction between endogenous CEP192 and AURKA, leading to the mitotic defects. Together, the results reveal distinct AURKA-CEP192 interactions that are different from other cofactors (e.g., TPX2) and can be further exploited for discovering potential AURKA inhibitors by modulating the interaction between CEP192 and AURKA.

RESULTS

CEP192 interacts AURKA with the conserved helix within AURKA-BD

Human CEP192 consists of the following domains: (i) a less well-conserved and predicted mostly unstructured N-terminal region containing AURKA-BD and (ii) a C-terminal domain containing tandem repeats of the PapD-like domains (Fig. 1A) (*22*, *23*). Using pull-down studies, it was previously shown that the *Xenopus laevis* CEP192 AURKA-BD (residues 543 to 747; AURKA-BD) interacts with the kinase domain of *X. laevis* AURKA (*6*, *7*). Here, we set out to specifically map and quantitatively characterize the interactions between the human CEP192 and AURKA.

Using ITC, N-terminal maltose binding protein (MBP)–tagged AURKA-BD of human CEP192 residues 440 to 631 (which corresponds to AURKA-BD of *X. laevis* AURKA-BD; fig. S1A) bound the kinase domain of AURKA (human AURKA residues 123 to 403) with low micromolar affinity [dissociation constant (K_d) = 1.2 ± 0.1 μM] and ~1:1 stoichiometry (Fig. 1B). Most of AURKA-BD of CEP192 is predicted to be unstructured; however, sequence analysis and structure prediction revealed regions of relatively high conservation that mostly coincide with α-helices (Helix-1, CEP192 residues 511 to 527; Helix-2, CEP192 residues 581 to 591) (fig. S1B) (*24*, *25*). To test whether these conserved helical segments participate in the interaction with AURKA, we made a series of purified MBP-tagged CEP192 recombinant proteins and tested their binding to $AURKA_{123–403}$. MBP-$CEP192_{456–541}$, in which the C-terminal region containing Helix-2 was deleted, bound $AURKA_{123–403}$, as shown by ITC (Fig. 1C). Furthermore, MBP-$CEP192_{491–541}$, which additionally lacks an unstructured N-terminal region, also bound $AURKA_{123–403}$ with low micromolar affinity (K_d = 1.9 ± 0.1 μM) and ~1:1 stoichiometry (Fig. 1D).

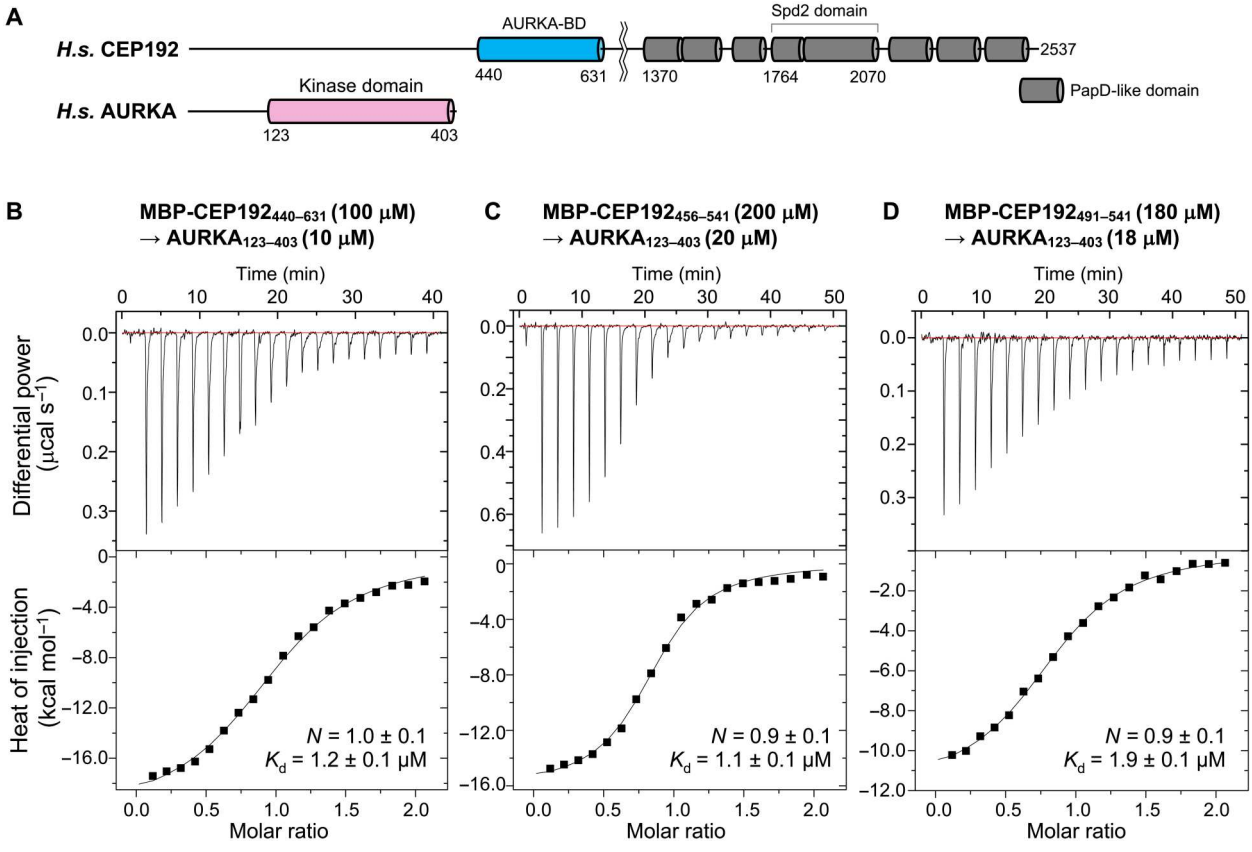

Fig. 1. Quantitative analysis of interactions between centrosomal protein of 192 kDa (CEP192) and Aurora kinase A (AURKA). (**A**) Domain organization of *Homo sapiens* (*H.s.*) CEP192 and AURKA. (**B** to **D**) Isothermal titration calorimetry (ITC) titrations of CEP192 and AURKA constructs as indicated. Listed with each titration are the concentrations of the protein in the syringe and in the cell, as well as the parameters of the fit (stoichiometry *N*, dissociation constant K_d). Errors correspond to the SD of the fits.

Having mapped AURKA interaction regions on CEP192 residues 491 to 541, we hypothesized that the conserved Helix-1 is the main determinant for binding to AURKA; then, we set out to further quantitatively map the interaction on CEP192 (Fig. 2A). MBP-CEP192$_{506–536}$, which extends several conserved amino acids beyond the N and C termini to Helix-1, bound AURKA$_{123–403}$ with low micromolar affinity (K_d = 3.0 ± 0.6 μM) (Fig. 2B). A synthetic peptide that corresponds to the same residues (CEP192 residues 506 to 536) bound AURKA$_{123–403}$ with similar affinity (K_d = 5.3 ± 0.6 μM) (fig. S2), indicating that MBP had almost no influence on the interaction. To more specificallymap the interaction, we generated three C-terminallytruncated constructs, MBP-CEP192$_{506–530}$, MBP-CEP192$_{506–527}$, and MBP-CEP192$_{506–524}$, and tested their binding to AURKA (Fig. 2, C to E). MBP-CEP192$_{506–530}$ and MBP-CEP192$_{506–527}$ both bound AURKA$_{123–403}$, albeit the latter construct showed a reduced binding affinity (K_d = 15.8 ± 1.4 μM), presumably due to the partial impairment of peptide folding (Fig. 2, C and D). Further truncating the three C-terminal three residues into the MBP-CEP192$_{506–527}$ construct completely abolished the binding (Fig. 2E). In a similar way, MBP-CEP192$_{509–527}$, in which the conserved residues at the N terminus of Helix-1 were removed, failed to bind AURKA$_{123–403}$ (Fig. 2F). Consistent with this observation,MBP-CEP192$_{506–536}$ F508S, in which the strictly conserved phenylalanine residue at the N terminus was mutated to serine, failed to bind AURKA (Fig. 2G). Together, these results conclusively show that the essential AURKA binding segment of human CEP192 is confined within CEP192 residues 506 to 536 and mainly consists of Helix-1.

CEP192$_{506–536}$ binds AURKA via a site distinct from TPX2 and is incapable of activating AURKA

The essential binding region of CEP192 shows very low sequence similarity with that of TPX2 (Fig. 3A) (*13*, *14*). This finding led us to hypothesize that CEP192 may have a different binding site on AURKA than TPX2 with distinct activation modes. To test this hypothesis, we established an FP-based competition assay. In our FP assay, the observed K_d value of fluorescein isothiocyanate (FITC)–labeled CEP192$_{506–536}$ and AURKA$_{123–403}$ was 0.7 μM, which was ~4-fold higher than that obtained from the ITC experiment (K_d = 3.0 ± 0.6 μM) (Figs. 2B and 3B). The difference in binding affinity could be attributed to the different experimental conditions [e.g., intrinsic sensitivity of each experiment (measuring fluorescence versus enthalpy) and different protein concentrations]. The affinity between FITC-labeled TPX2$_{1–43}$ and AURKA$_{123–403}$ (K_d = 0.5 ± 0.1 μM) (Fig. 3B) measured with FP was consistent with previous reports (*13*, *26*). The observed affinity between TPX2$_{1–43}$ and AURKA$_{123–403}$ is similar to that between FITC-CEP192$_{506–536}$ and AURKA$_{123–403}$, suggesting that TPX2 and CEP192 could compete with each other (at least in vitro), if they have the same binding site on AURKA$_{123–403}$.

The nonlabeled CEP192$_{506–536}$ peptide was able to displace FITC-labeled CEP192$_{506–536}$ from binding to AURKA, as expected [half-maximal inhibitory concentration (IC_{50}) = 21.0 ± 5.7 μM] (Fig. 3C), while the same nonlabeled peptide was not able to displace FITC-labeled TPX2$_{1–43}$ peptide from AURKA binding (Fig. 3D). These results suggest that AURKA may interact with CEP192 through different binding sites than those observed in AURKA-TPX2 complex structures (*13*, *14*). We further tested whether the addition of CEP192$_{506–536}$ peptide can stimulate the kinase activity of AURKA, similar to TPX2$_{1–43}$ peptide. Previously, binding of TPX2$_{1–43}$ peptide has been shown to allosterically activate the kinase activity of AURKA regardless of its phosphorylation state by inducing structural transition toward the DFG-in state and stabilizing the catalytically active AURKA conformation (*12*, *13*, *15*, *27*). TPX2 binding enhances the kinetics of the kinase reaction of phosphorylated AURKA [~2- to 3-fold increase in initial velocity and K_{cat} (turnover number)] as well as dephosphorylated AURKA (~5-fold increase in initial velocity and ~50-fold increase in K_{cat}) (*13*, *15*, *28*, *29*). In addition, TPX2 binding increases the overall adenosine triphosphate (ATP) hydrolysis and the amount of adenosine diphosphate (ADP) produced in a certain reaction period by AURKA (*30*). However, although it is necessary for CEP192 to bind AURKA for the activation of AURKA, the binding of AURKA-BD itself is not sufficient to activate the kinase (*6*, *7*).

To investigate the impact of TPX2 or CEP192 binding on AURKA activity, we purified three different forms of AURKA: bacterially expressed, phosphorylated AURKA$_{123–403}$WT, phosphorylated AURKA$_{123–403}$C290,393A, and dephosphorylated AURKA$_{123–403}$C290,393A (fig. S3; note that we used AURKA$_{123–403}$C290,393A mutant to prepare the dephosphorylated version of AURKA, as the mutant is more stable and less susceptible to autophosphorylation) (*13*, *31*). See Materials and Methods for detailed protein preparation procedure. Bacterially expressed, phosphorylated AURKA$_{123–403}$C290,393A showed comparable activity compared to wild type (WT), consistent to previous observations (*15*, *32*), while dephosphorylated AURKA$_{123–403}$C290,393A showed marginal activity, only at 300 nM concentration (Fig. 3E). When we measured the kinase activity by quantifying the amount of ADP produced by 30 nM AURKA using the ADP-Glo kinase activity assay, we observed that the addition of TPX2$_{1–43}$ peptide activated the phosphorylated AURKA$_{123–403}$WT, as well as the phosphorylated AURKA$_{123–403}$C290,393A and dephosphorylated AURKA$_{123–403}$C290,393A (Fig. 3, F to H). However, the CEP192$_{506–536}$ peptide and the N-terminal half-fragment of CEP192$_{1–995}$ [the fragment that can recruit pericentriolar material (PCM) proteins (*7*)] were unable to activate the kinase activity of all three forms of AURKA (Fig. 3, F to H). To further test whether CEP192 binding alone is insufficient to promote the autophosphorylation of AURKA, we performed Western blotting using an anti–phospho-Thr^{288} (pT288) AURKA antibody with dephosphorylated AURKA$_{123–403}$C290,393A to directly probe the autophosphorylation state of AURKA upon TPX2 or CEP192 binding. The addition of TPX2$_{1–43}$ peptide led to an increase in the autophosphorylation of the dephosphorylated AURKA$_{123–403}$ C290,393A mutant, as indicated by increased levels of pT288 on Western blot analysis (fig. S4A). However, CEP192$_{506–536}$ and CEP192$_{1–995}$ were not able to promote the autophosphorylation of dephosphorylated AURKA$_{123–403}$C290,393A (fig. S4, B and C).

Together, the results suggest that CEP192$_{506–536}$, which contains an essential AURKA binding site, binds AURKA at a binding site distinct from that of TPX2, and the binding of this essential fragment is not sufficient to activate the autophosphorylation and transphosphorylation activity of AURKA.

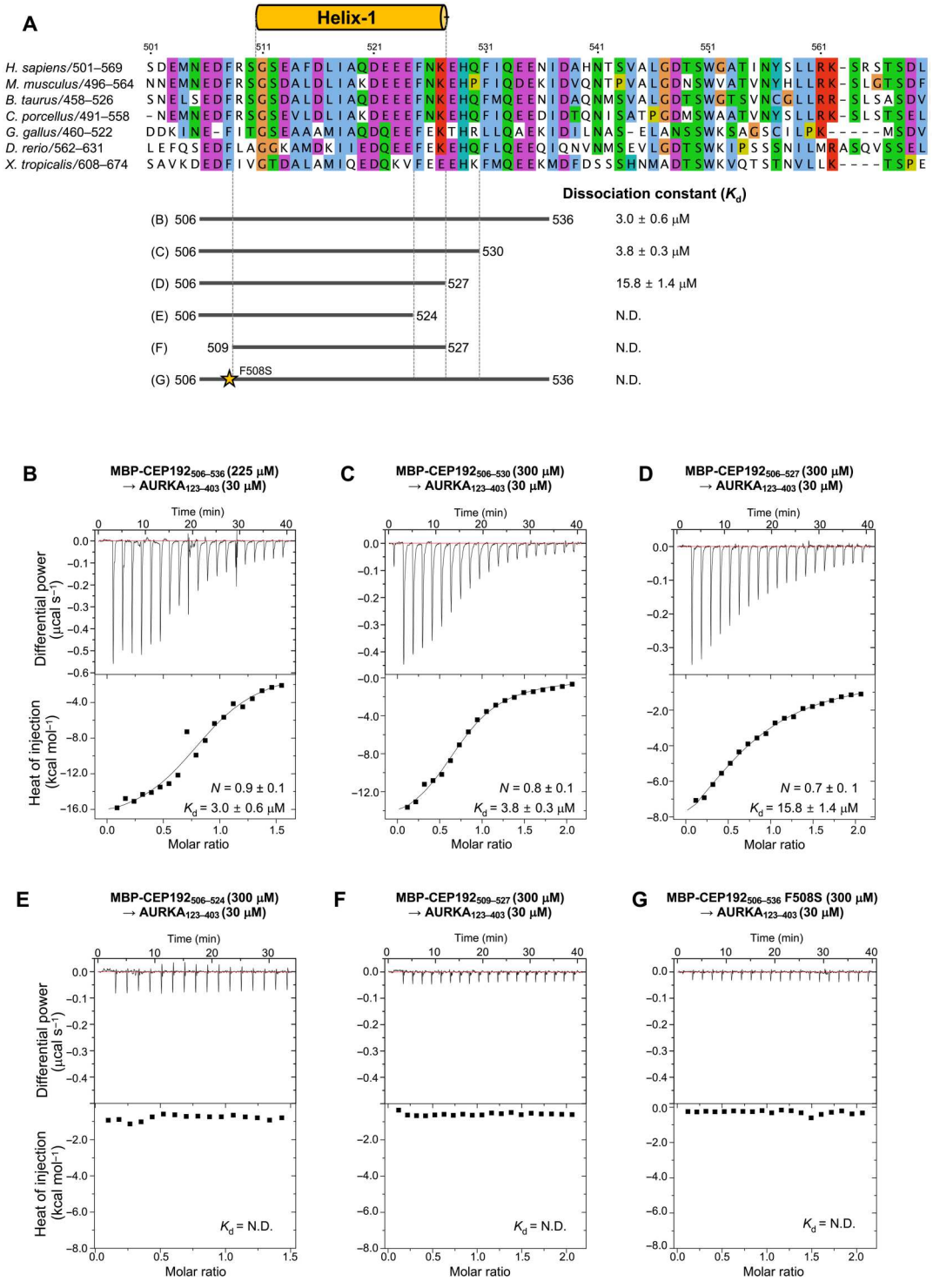

Fig. 2. The conserved Helix-1 within AURKA-binding domain (AURKA-BD) of centrosomal protein of 192 kDa (CEP192) binds the kinase domain of AURKA. (**A**) Alignment of CEP192 sequences from different species [*Homo sapiens* (UniProt ID: Q8TEP8), *Mus musculus* (UniProt ID: E9Q4Y4), *Bos taurus* (UniProt ID: A0A3Q1LJH6), *Cavia procellus* (UniProt ID: H0V7I4), *Gallus gallus* (UniProt ID: A0A1D5PSP1), *Danio rerio* (UniProt ID: A0A0R4IEX1), and *Xenopus tropicalis* (UniProt ID: A0A6I8S9H5)] around Helix-1 within AURKA-binding domain (AURKA-BD) (top) and domain diagram showing the constructs used in the Isothermal titration calorimetry (ITC) experiments (bottom). (**B** to **G**) ITC titrations of maltose binding protein (MBP)–CEP192 constructs (as indicated) into $AURKA_{123–403}$. Listed with each titration are the concentrations of the protein in the syringe and in the cell, as well as the parameters of the fit (stoichiometry *N*, dissociation constant K_d). Errors correspond to the SD of the fits.

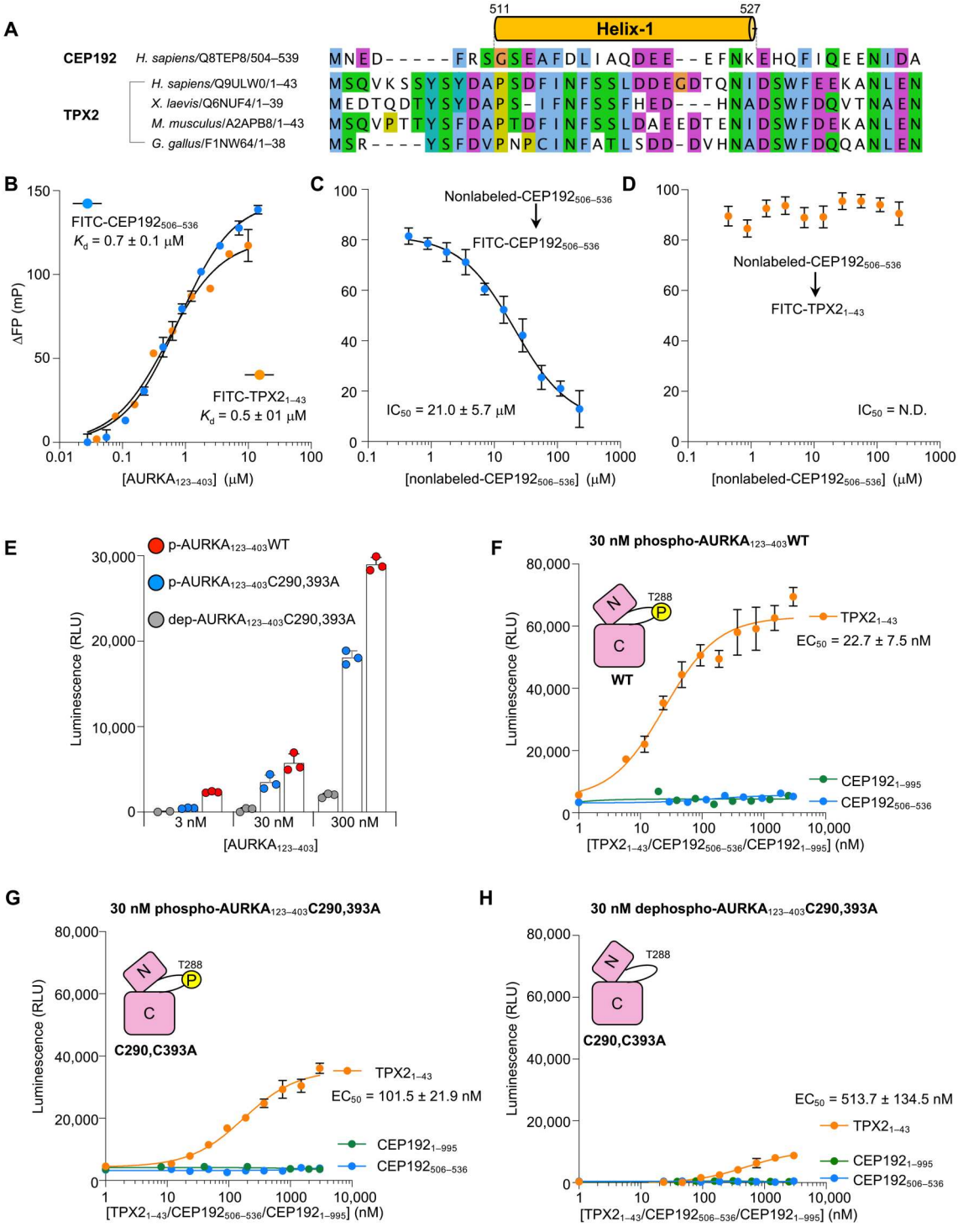

Fig. 3. Centrosomal protein of 192 kDa (CEP192) binds to a distinct region of Aurora kinase A (AURKA), and the binding by itself cannot activate AURKA. (**A**) Alignment of CEP192 sequences around the predicted conserved helix (Helix-1) and targeting protein for Xklp2 (TPX2) sequences from different species (UniProt accession codes are listed with the name of each sequence). (**B**) Binding affinities of $CEP192_{506–536}$ (blue) and $TPX2_{1–43}$ (orange) to $AURKA_{123–403}$ determined with fluorescence polarization (FP) assays. The errors correspond to the SD from triplicate measurements. (**C** and **D**) Competitive binding inhibition assay. FITC-labeled $CEP192_{506–536}$ (C) or FITC-labeled $TPX2_{1–43}$ (D) in complex with $AURKA_{123–403}$ (1 μM) is displaced by nonlabeled $CEP192_{506–536}$. The errors correspond to the SD from triplicate measurements. (**E**) In vitro kinase assay (ADP-glo assay) showing kinase activities of phosphorylated $AURKA_{123–403}$wild type (WT) (red), phosphorylated $AURKA_{123–403}$C290,393A (blue), and dephosphorylated $AURKA_{123–403}$C290,393A (gray) at indicated concentrations (3, 30, and 300 nM). (**F** to **H**) In vitro kinase assay [adenosine diphosphate (ADP)–glo assay] showing stimulation of kinase activity of (F) 30 nM phosphorylated $AURKA_{123–403}$WT, (G) 30 nM phosphorylated $AURKA_{123–403}$C290,393A, and (H) 30 nM dephosphorylated $AURKA_{123–403}$C290,393A by $TPX2_{1–43}$ (orange), $CEP192_{506–536}$ (blue), or $CEP192_{1–995}$ (green). The errors correspond to the SD from triplicate measurements. N.D., not determined; RLU, relative light unit.

Crystal structure of a chimeric CEP192$_{506–527}$-AURKA$_{123–403}$ provides structural insights into their interaction

To further understand the structural mechanism of the interaction between AURKA and CEP192, we set out to determine the crystal structure of human AURKA$_{123–403}$ in complex with essential AURKA binding segment of CEP192. Unfortunately, our numerous attempts to obtain AURKA in complex with various CEP192 peptides yielded only apo AURKA$_{123–403}$ crystals without any extra electron density that corresponds to CEP192; this result was possibly due to the crystal packing interactions that precluded the peptide from AURKA binding site during the crystallization process. Therefore, we generated chimeric constructs with AURKA in which the N-terminal region of full-length AURKA (residues 1 to 122) was removed and replaced with various CEP192 constructs. We also mutated solvent-exposed cysteine residues of AURKA (Cys^{290}, Cys^{393} to Ala) to enhance the stability of the protein (*31*, *32*). Among the various chimeric proteins created with different linker lengths, only the CEP192$_{506–527}$-fused AURKA$_{123–403}$C290,393A mutant without any extra linker residues, which we refer to with the term "CEP192-AURKA$_{chimera}$," produced diffraction-quality crystals. Although there are no linker residues, the N terminus of AURKA$_{123–403}$ (^{123}SKKR^{126}) and the C terminus ofCEP192$_{506–527}$ (^{526}NK^{527}) contain flexible residues, forming a flexible region of six amino acids at the junction: ^{121}NKSKKR^{126}. The electron density for this region is weak and shows structural diversity between chains (see below). Therefore, we speculate that this flexible region would provide structural flexibility for the native interactions between the two fused proteins.

Unexpectedly, CEP192-AURKA$_{chimera}$ was trimeric in solution, as analyzed by multiangle light scattering (Fig. 4A). This suggests that the chimeric molecules may engage in intermolecular interactions, leading to the formation of nonnative trimeric assembly that might have aided the crystallization.

The crystals of CEP192-AURKA$_{chimera}$ diffracted to 2.7 Å, and we determined the structure by molecular replacement using the apo AURKA kinase domain [Protein Data Bank (PDB) ID: 5DT3] as a search model (table S1). The orthorhombic crystals, which belong to the space group $P2_12_12_1$, contain three chimeric molecules in each asymmetric unit, and this result was consistent with the observed trimeric assembly in solution. In our crystal structure, the CEP192 region of the chimeric protein interacts intermolecularly with the adjacent neighboring N-terminal region of AURKA, creating pseudo-threefold symmetry and explaining why the protein is trimeric in solution (Fig. 4, A and B). In addition, the activation segments were also engaged in domain-swapped interactions, as similarly seen in a previous report (*13*) (fig. S5, A and B). We observed identical interactions stabilizing domain-swapped conformations between W313 (from one monomer) and P297 and P298 (from a neighboring monomer) and interactions between R371 (from one monomer) and E299 (from a neighboring monomer) in CEP192-AURKA$_{chimera}$ (fig. S5, C and D). Although CEP192-AURKA$_{chimera}$ formed the unexpected domain-swapped interactions and nonnative trimeric assembly, the interactions observed within the CEP192 and AURKA interface were functionally relevant, as shown in the mutational analysis (see below).

The electron density of CEP192-AURKA$_{chimera}$ corresponding to AURKA kinase domain was well defined except for the portion of activation segments, the C-terminal residues, and the junction between CEP192 and AURKA, suggesting the flexibility of those regions (fig. S6A). The electron density of the CEP192 region is clearly visible in nearly all residues in all chains (fig. S6A). When we compared the structures of chains A, B, and C, all three chains showed almost identical structures [root mean square deviations (RMSDs) of 0.3 to 0.7 Å between equivalent Cα atoms among the kinase domain of all chains; RMSDs of 0.6 to 1.0 Å between equivalent Cα atoms among the CEP192 region of all chains] and intermolecular interactions, except for the junction region linking CEP192 and AURKA (fig. S6, B to D). Therefore, we only describe the structures of the CEP192 region from chain A and the AURKA region from chain B and their interactions for simplicity, unless otherwise indicated (Fig. 4B).

CEP192 Helix-1 binds to a distinct surface on AURKA, compared to TPX2

The CEP192 region of CEP192-AURKA$_{chimera}$ extends outward, docks onto a neighboring AURKA N-lobe, and wraps around to bind to the top of AURKA N-lobe, which consists of β-strands β1 to β3, distinct from the previously well-characterized TPX2 binding pocket (Fig. 4C). The minimal AURKA-BD of TPX2 (residues 1 to 43) interacts mainly with AURKA's three hydrophobic pockets: Y-[which is analogous to the PDK1-interacting fragment (PIF) pocket], F-, and W-pockets (*33*, *34*). The observed CEP192 binding surface of AURKA is totally distinct from the TPX2 binding site, explaining why the CEP192 peptide was incapable of displacing TPX2$_{1–43}$ from AURKA binding (Fig. 3D).

The interactions between CEP192 and AURKA are mediated by both extensive hydrophobic and hydrophilic interactions, contrary to the interactions between AURKA and TPX2, which are predominantly mediated by the hydrophobic interactions (*13*, *14*). As expected, AURKA-bound CEP192 mostly adopts an α-helical structure (Helix-1; S512-N526), with a short loop (E506-G511) at the N terminus (Fig. 4, C and D). The six residues comprising the N-terminal short loop region (506-EDFRSG-511) run along one side of the shallow groove formed by the residues on β1 and β3 of AURKA and partially overlap with the AURKA-bound TACC3 structure (Fig. 4E) (*35*). Among the interacting residues on the CEP192 side, F508 seems to play a key role, by inserting deeply into a hydrophobic groove formed by residues I158 and L149 of AURKA, as similarly seen in the TACC3-AURKA structure (Fig. 4E). In the TACC3-AURKA structure, TACC3 residue F525 is also inserted into the same hydrophobic pocket (*35*). This explains why the mutant MBP-CEP192$_{F508S}$ failed to bind AURKA$_{123–403}$ (Fig. 2G). The interactions are further strengthened by the hydrophilic interactions between E506 and R509 (CEP192 residues) and R137 and I135 (AURKA residues) (Fig. 4E). The succeeding Ser^{509}-Gly^{510}-Ser^{511} residues act as a flexible hinge, directing the following α-helical structure toward the top surface of AURKA N-lobe (Fig. 4E).

An overlap between the TACC3 and CEP192 binding sites on AURKA is particularly interesting, as it suggests that TACC3 and CEP192 can compete for AURKA binding with each other, as seen in the other cofactor pair, Bora and TPX2. Bora and TPX2 compete with each other for the binding to AURKA in vitro, and the level of Bora has been suggested to control the availability of AURKA in interactions with TPX2 in human cells (*30*, *36*). Analogously, the competition between TACC3 and CEP192 might also have important implications in the context of AURKA regulation in the centrosome, as these cofactors have different binding and

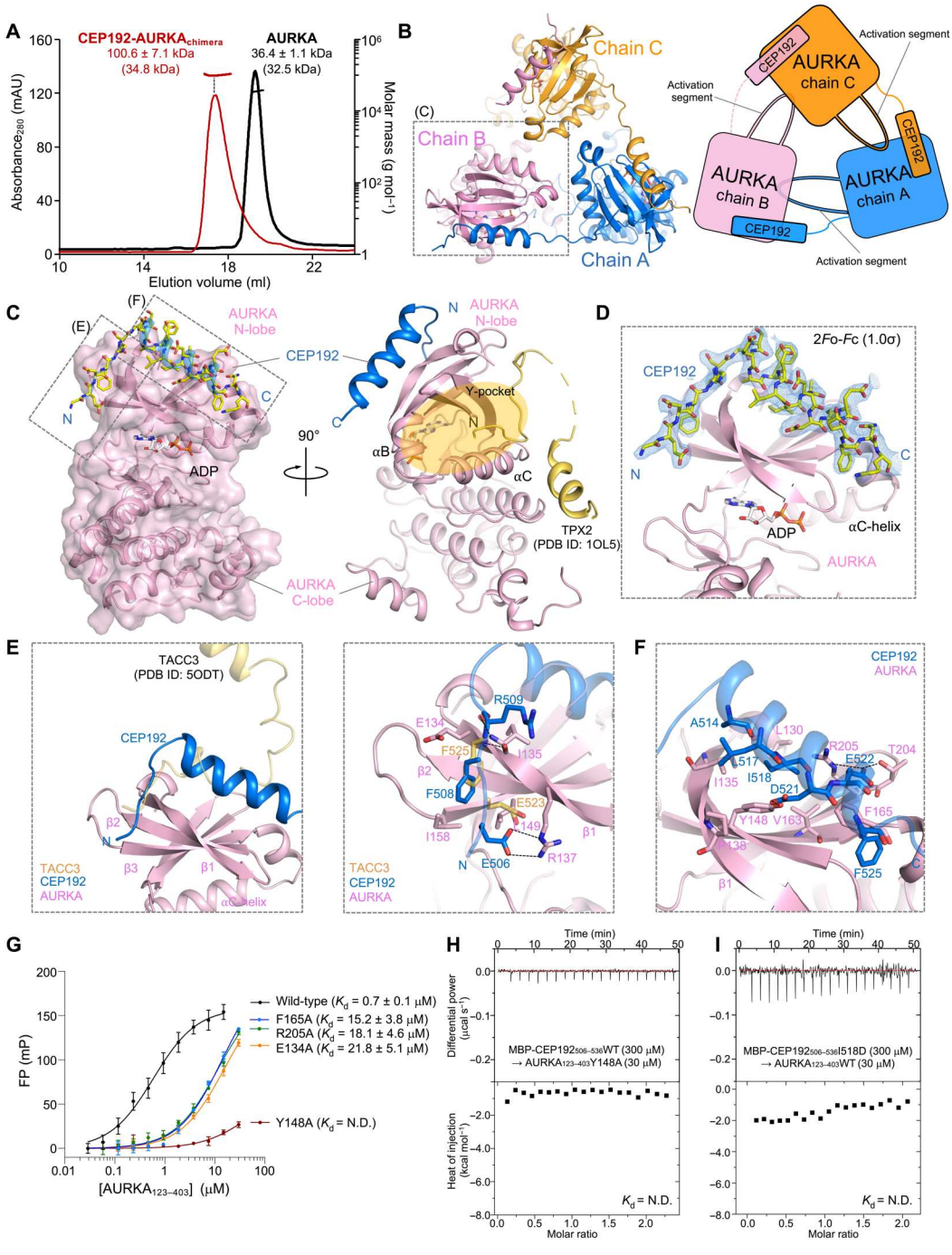

Fig. 4. Crystal structure of centrosomal protein of 192 kDa (CEP192)–Aurora kinase A (AURKA)$_{chimera}$. (**A**) Size exclusion chromatography–multiangle light scattering analysis of CEP192-AURKA$_{chimera}$ and AURKA$_{123–403}$. The molar mass (right *y* axis) and the UV$_{280nm}$ (left *y* axis) are plotted. The theoretical masses are given in parentheses. (**B**) Left: Ribbon representation of the structure of CEP192-AURKA$_{chimera}$ (colored as blue, pink, and orange for chains A, B, and C, respectively). Right: Schematic representation showing trimeric assembly of the protein. (**C**) Ribbon representation of CEP192-AURKA$_{chimera}$ structure, from the boxed region in (B). CEP192 region is colored in blue, and the side chains are shown using a stick representation that is colored by atom type. AURKA region is colored in pink, and the surface is shown. Targeting protein for Xklp2 (TPX2)–complexed AURKA structure (PDB code: 1OL5) is superimposed, and TPX2 is shown in yellow. (**D**) Close-up view of the CEP192 binding site, showing the 2*Fo-Fc* electron density map (blue mesh) at 2.7-Å resolution contoured at 1 σ around an all-atom representation of CEP192 region. (**E**) Close-up view of the short loop (E506–G511) of the CEP192 binding site from the boxed region in (C), which overlaps the TACC3 binding site. Left: The TACC3-complexed AURKA structure (PDB code: 5ODT) is superimposed, and TACC3 is shown in yellow. Right: Residues involved in the interaction between CEP192 and AURKA. TACC3 residues F525 and E523 are also shown in yellow sticks. The hydrogen bonding interactions are shown as dotted lines. (**F**) Close-up view of the conserved helix (Helix-1) binding site, from the boxed region in (C). Hydrogen bonding interactions are shown (dotted lines). (**G**) Fluorescence polarization (FP) measurements of the indicated AURKA mutants binding into FITC-CEP192$_{506–536}$. Errors correspond to the SD from triplicate measurements. (**H**) Isothermal titration calorimetry (ITC) titration of the MBP-CEP192$_{506–536}$ into AURKA$_{123–403}$Y148A mutant. (**I**) ITC titration of the MBP-CEP192$_{506–536}$I518D mutant into AURKA$_{123–403}$.

activating capabilities that would help AURKA to more precisely control its multiple functions depending on a specific cellular context.

The α-helical region of CEP192 (S512-N526) has extensive interactions with AURKA, including both hydrophobic and hydrophilic interactions (Fig. 4F). Hydrophobic interactions occur between residues from Helix-1 A514/L517/I518/F525 with the residues on the top surface of AURKA N-lobe. Specifically, I518 inserts into a hydrophobic pocket surrounded by AURKA's four aliphatic amino acid side chains (L130, I135, Y148, and V163), and the phenyl side chain of F525 from CEP192 and F165 from AURKA participates in pi-pi stacking interactions (Fig. 4F). Beyond hydrophobic interactions, CEP192 Helix-1 uses D521 and E522 side chains to make hydrogen bonds with the side chains of Y148 and R205/

T204 of AURKA, respectively (Fig. 4F). As a whole, CEP192 snakes around the top side of the N-terminal part of AURKA, distinct from TPX2 binding sites.

To confirm that the observed interactions in the crystal structure represent a true native binding site and not an artifact of using the chimeric protein for crystallization, we mutated several aforementioned key residues on both sides of the complex in the crystal structure and tested the binding affinity. AURKA mutations E134A, F165A, R205A, and Y148A within the CEP192 binding interface all resulted in a marked decrease in binding toward FITC-labeled $CEP192_{506–536}$ as shown by FP, demonstrating that the residues mutated play a key role in the interactions (Fig. 4G). We further verified the interaction between AURKA Y148A and $CEP192_{506–536}$ using another method (i.e., ITC) and observed no binding (Fig. 4H). In contrast, AURKA single-mutant W128A or double-mutant Y246/V252A (residues on AURKA-TPX2 binding interface) retains almost the same binding affinity toward FITC-labeled $CEP192_{506–536}$, providing further evidence that the interaction between AURKA-CEP192 is distinct from that between AURKA-TPX2 (fig. S7).

In addition to the aforementioned CEP192 F508S, which failed to bind AURKA (Fig. 2G), we also mutated I518 on the CEP192 side of the complex and tested the binding toward AURKA by ITC (note that we used ITC instead of FP when testing CEP192 mutation on binding affinity, as FP requires fluorescent-labeled synthetic CEP192 peptides, which are costly and involve a time-consuming procedure for peptide synthesis). The resulting MBP-CEP192 I518D failed to bind AURKA, further confirming that the observed interactions in the crystal structure are true native binding interactions (Fig. 4I).

Collectively, these results confirm that CEP192 adopts a short loop (E506-S509) followed by an α-helical structure (Helix-1; S512-N526) that wraps around AURKA N-terminal surface formed by the residues mostly on β1 to β3, which is distinct from TPX2 binding sites.

Another interesting feature observed in our structure is the inactive conformation of CEP192-bound AURKA. The active conformation of AURKA (e.g., TPX2 or N-myc bound) has characteristic structural hallmarks, such as DFG-in, "C-helix in," and the formation of a "Glu-Lys salt bridge (Glu^{181}-Lys^{162})," which exists simultaneously (*37*). In contrast, the αC-helix of CEP192-bound AURKA is rotated out (referred to as "C-helix out"), and Glu^{181} and Lys^{162} are unable to form a salt bridge (Fig. 5). However, we are cautious about interpreting the features of inactive conformations observed in our AURKA-$CEP192_{chimera}$ structure because (i) AURKA, especially its activation segment, is unusually flexible, allowing several populations of inactive and active populations to exist in a dynamic structural equilibrium in solution (*38*, *39*), and (ii) several experimental factors, such as crystal packing interactions, the use of a chimeric protein for crystallization, and the observed domain swapping interactions, could have affected the conformation of AURKA captured in our CEP192-$AURKA_{chimera}$ structure. It is worth noting, however, that these structural observations are consistent with (i) our biochemical assays demonstrating that CEP192 binding is not able to activate AURKA (Fig. 3, F to H, and fig. S4) and (ii) the previous work that has shown that the recombinant CEP192 (*6*, *7*) is also incapable of activating the kinase in the absence of the centrosome (or other factors that can mediate oligomerization such as αAURKA/αCEP192 antibody–coated beads).

AURKA-CEP192 Helix-1 interaction is crucial for AURKA activity in cells

Having biophysically and structurally validated the interactions between CEP192 Helix-1 and AURKA, we next assessed the functional significance of the interactions in cells. As CEP192 mediates AURKA localization to the centrosome and activation is essential for the proper centrosome separation and bipolar spindle assembly, abrogation of the CEP192-AURKA interaction in cells leads to a malformed spindle and defects in centrosome separation. Previously, exogenous addition of AURKA-BD of *X. laevis* CEP192 (residues 521 to 757) displaced the endogenous *X. laevis* AURKA-CEP192 interactions in metaphase-arrested Xenopus egg extract and prevented the localization and activation of AURKA in a dominant negative fashion (*6*). Furthermore, human CEP192 lacking AURKA-BD (residues 436 to 634) could not rescue the mitotic defects in endogenous CEP192-depleted HeLa cells, suggesting the critical role of AURKA-BD and CEP192 interactions in mammalian cells (*7*). Here, we further specifically assessed the functional importance of CEP192 Helix-1 and AURKA interactions in cells, which we characterized through biophysical and structural methods.

To test the importance of CEP192 Helix-1–AURKA interactions in cells, we overexpressed human GFP-$CEP192_{506–530}$WT as well as mutant (GFP-$CEP192_{506–530}$F508S) in HeLa cells that were synchronized at G_2-M phase by nocodazole treatment and analyzed using immunofluorescence (fig. S8). As GFP-$CEP192_{506–530}$ should compete with endogenous CEP192 for binding to AURKA, GFP-$CEP192_{506–530}$ could be expected to function as a dominant-negative factor, while GFP-$CEP192_{506–530}$F508S, which is a peptide that carries the mutation found to inhibit binding of CEP192 to AURKA (Fig. 2G), cannot work as dominant-negative factor. Compared to the expression of green fluorescent protein (GFP) alone (Fig. 6A, panel "Control"), we observed a marked increase in spindle orientation and assembly defects [which are characteristics of CEP192 knockdown and abrogation of CEP192-AURKA interactions (*7*, *40*)] when GFP-$CEP192_{506–530}$WT was expressed, indicating that $CEP192_{506–530}$WT competes with endogenous CEP192, leading to abnormal spindle assembly (Fig. 6, A and B). Compared to the expression of GFP-$CEP192_{506–530}$WT, the expression of GFP-$CEP192_{506–530}$F508S altered the cellular phenotypes to a much less degree (Fig. 6, A and B). Also, in cells with a bipolar spindle, we observed that the expression of GFP-$CEP192_{506–530}$WT decreased the intercentrosomal distances, which is a characteristic CEP192 knockdown phenotype (Fig. 6C) (*7*). In contrast, the expression of GFP-$CEP192_{506–530}$F508S had no effect on the intercentrosomal distances. Together, these results show that the CEP192-AURKA interaction that is mainly mediated by CEP192 Helix-1, and more specifically CEP192 residue F506, is absolutely necessary for the proper CEP192-mediated AURKA activation process at the centrosome in mammalian cells.

DISCUSSION

AURKA plays diverse and critical functions throughout the cell cycle, especially in mitosis, necessitating spatially and temporally

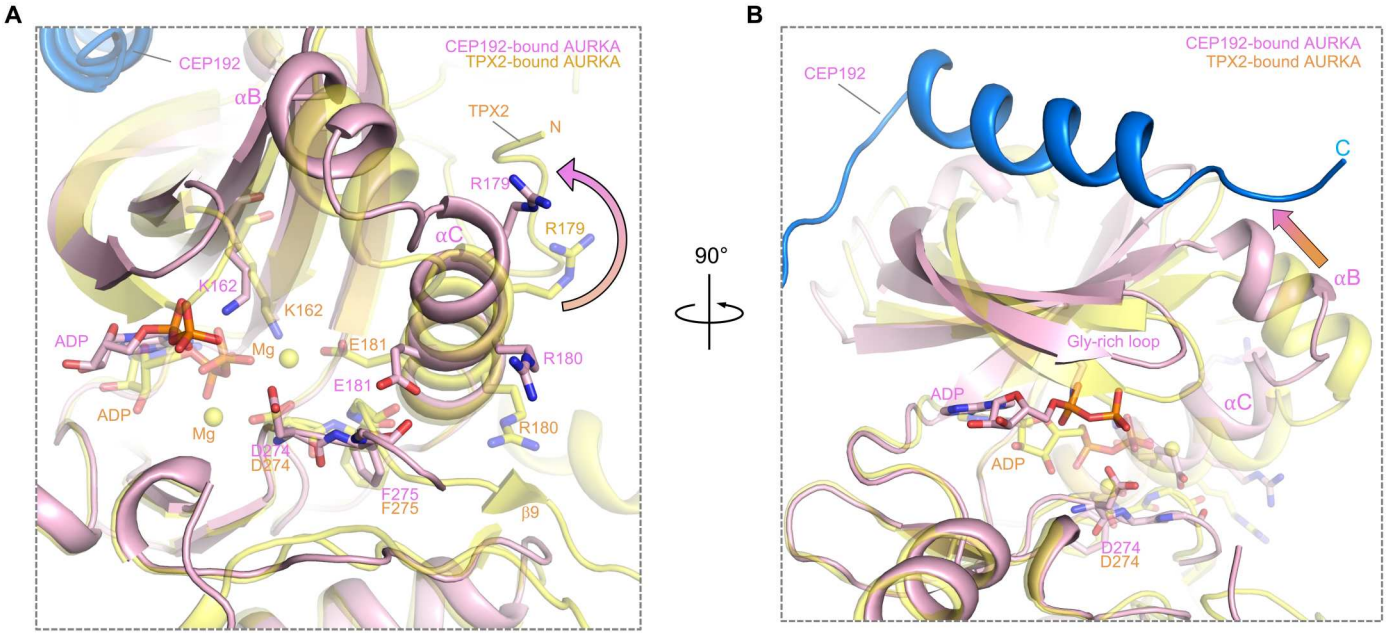

Fig. 5. Aurora kinase A (AURKA) displays an inactive conformation when bound to centrosomal protein of 192 kDa (CEP192). (**A** and **B**) Superimposition of the structure of $AURKA_{123–403}$ from the CEP192-$AURKA_{chimera}$ (pink) and targeting protein for Xklp2 (TPX2)–bound complex (yellow; PDB ID: 1OL5).

coordinated activation and regulation (*1*, *2*, *41*). How AURKA can be regulated to control such a diverse set of processes remains a fundamental question. It is now widely accepted that the functional diversity of AURKA depends on the intramolecular and intermolecular factors, including phosphorylation, oxidation, and interactions with the cofactor proteins (*3*, *42*–*45*). Although TPX2 and CEP192 have been regarded as two major AURKA cofactors that regulate the activity and localization of AURKA (*3*), the extensive efforts performed over the two decades have mostly focused on TPX2. Therefore, much less is known about the CEP192-mediated AURKA regulation. Here, we shed light on the structural basis for the CEP192-mediated AURKA regulation through the biophysical, structural, and cellular approaches.

In our crystal structure, CEP192 Helix-1 binds AURKA on the surface, which is different from the TPX2 binding site (*13*, *14*) but involves a similar binding affinity (Fig. 3B). CEP192 binding not only occurs at the distinct binding site on AURKA but also elicits different functional responses. TPX2 binding evokes substantial conformational rearrangements, and the binding itself is sufficient to transform AURKA into the catalytically active state (*14*). In contrast, the binding of CEP192 cannot activate AURKA in vitro (Fig. 3, F to H), in *Xenopus* egg extract, and in mammalian cells, regardless of N-terminal half-fragment that can recruit other PCM proteins or minimal fragment for binding (*6*, *7*). In this regard, CEP192 seems to act as a scaffold with a somewhat analogous function to the inner centromere protein (INCENP) that regulates the localization and activity of Aurora kinase B (AURKB), which shares ~60% identity with AURKA (*46*–*48*). INCENP, the platform on which the chromosomal passenger complex (CPC) that comprises AURKB, borealin, and survivin assembles, has been shown to activate AURKB through a multistep process (*46*, *49*). The binding of INCENP to the N-lobe of AURKB has only a marginal effect on the AURKB activation by itself and is insufficient to fully activate the kinase. The second step involves the transphosphorylation of Thr^{232} on AURKB (*50*, *51*). Therefore, the enrichment in CPC at specific cellular compartments facilitates the autophosphorylation of AURKB in trans and leads to the full activation of the kinase. These local density–dependent activation mechanisms may also be applied to the activation of CEP192-mediated AURKA activation.

Through the interaction with CEP192, AURKA localizes to the centrosome, leading to an elevated local concentration at the centrosome (*3*). In G_2 phase, PLK1 phosphorylates PCNT and phosphorylated PCNT subsequently mediates the centrosomal recruitment of CEP192 (*3*). The C-terminal part of CEP192, which contains PapD/Aspm-SPD2-Hydin (ASH) domains, might play a role in CEP192 localization to the centrosome, as mutations in the PapD/ASH domain have been shown to impair the centrosomal localization of CEP192 and its homolog in *Caenorhabditis elegans* [spindle-defective protein 2 (SPD-2)] (*52*–*54*). In the absence of the centrosome on which the C-terminal PapD/ASH domain of CEP192 can dock, CEP192 binding cannot activate the kinase, as CEP192 binding itself cannot activate the kinase or mediate oligomerization. In the presence of the centrosome [or other factors that can mediate oligomerization such as αAURKA/αCEP192 antibody–coated beads (*6*, *7*)], CEP192 can mediate a local concentration increase and activation of AURKA (fig. S9). The increased concentration of AURKA at the centrosome would facilitate the oligomerization of the kinase, subsequently promoting AURKA trans-autophosphorylation (*6*, *7*, *55*, *56*). After the recruitment to the centrosome by CEP192, the activity of AURKA can be further facilitated by its downstream kinase PLK1 (*57*) or through the inhibition of phosphatases (*58*). In G_2 phase, AURKA-PLK1 kinase cascade that promotes the G_2-M transition is initiated by CEP192 complexes at the centrosome or by Bora in the cytoplasm (*59*–*61*). As Bora binds to the same AURKA region that is used by

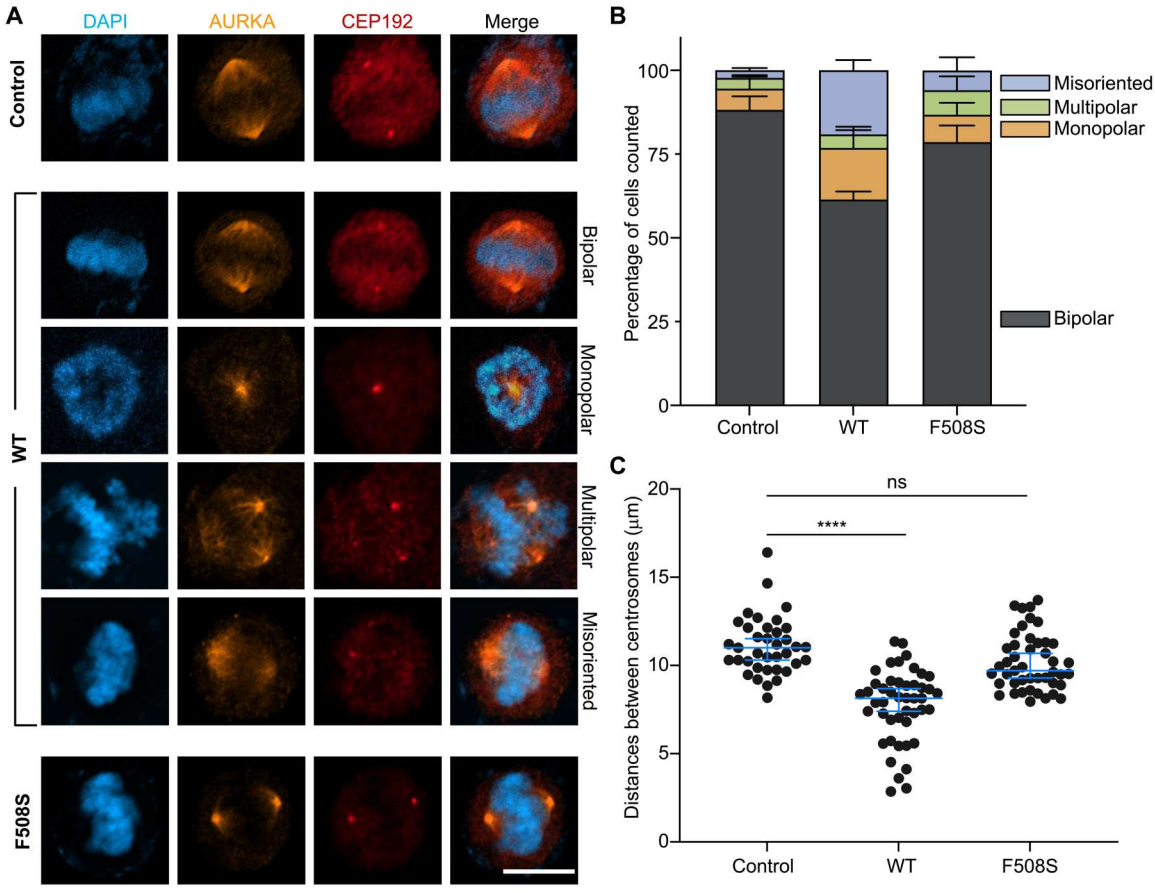

Fig. 6. Abrogation of the interaction between centrosomal protein of 192 kDa (CEP192) conserved helix (Helix-1) and Aurora kinase A (AURKA) leads to the mitotic defects. (**A**) Examples of immunofluorescence confocal images of the HeLa cells transfected with pEGFP-C1-empty vector (control), pEGFP-C1-CEP192$_{506–530}$WT, or pEGFP-C1-CEP192$_{506–530}$F508S constructs. The cells were stained with anti-AURKA (orange), anti-CEP192 (red) antibodies, and Hoechst 33342 (blue). Scale bar, 10 μm. Data shown are representative of three biological replicate experiments. (**B**) Quantification of mitotic phenotypes shown in (A). Bars represent mean values ± SEM of $n = 3$ biological replicate experiments. Approximately 100 cells were quantified for each condition. (**C**) Intercentrosomal distances between centrosomes marked with anti-CEP192 antibody in cells with a bipolar spindle. The statistical significance of the measurements was determined using the Kruskal-Wallis test, followed by a Dunn's multiple comparisons test; $n = 37$ (control), $n = 46$ [wild type (WT)], and $n = 45$ (F508S) cells. Bars indicate means ± SEM; ns, not significant; ****$P \leq 0.0001$.

TPX2 (*30*), CEP192 binding to AURKA is expected to not directly compete with the Bora binding to AURKA. Further work will be necessary to fully understand the interplay between AURKA, Bora, and CEP192 in G_2 phase.

AURKA has been found to be overexpressed in many different types of malignancies, making AURKA a promising therapeutic target in cancer treatment (*62*). The structure of CEP192-AURKA$_{chimera}$ presented in this study provides structural insights into the design of modulators of AURKA-CEP192 protein-protein interactions (PPIs). Recently, various noncatalytic functions of AURKA have been discovered, necessitating the development of modulators of the noncatalytic functions of AURKA to fully block AURKA in cancer (*63*, *64*), and the development of PPI blockers can be a promising strategy to modulate the noncatalytic function of AURKA (*65*). To date, the strategies to inhibit AURKA function by modulating the interaction between AURKA cofactors have been heavily focused on targeting interfaces between AURKA and TPX2, including the Y-pocket that is analogous to the PIF pocket (*26*, *33*, *66*–*68*). Although several small-molecule inhibitors that modulate AURKA-TPX2 interaction have been developed, AURKA that bound with those small molecules still displays hallmarks of an active kinase (i.e., DFG-In and K162-E181 salt bridge) (*33*, *67*). Therefore, AURKA might remain active in cells even when bound to those inhibitors. Also, as binding of TPX2$_{1–43}$ by itself activates AURKA, the TPX2 peptidomimetic cannot be used for therapeutic purposes (*26*). In this regard, the interface between CEP192 and AURKA might have better therapeutic potential, as CEP192 binding itself is insufficient to transform AURKA into the active state. Notably, a peptide mimicking CEP192 Helix-1 can be a great starting point for developing inhibitors targeting interactions between AURKA and CEP192, although whether the PPI between AURKA and CEP192 is druggable remains to be elucidated.

MATERIALS AND METHODS

Cloning, expression, and purification of recombinant proteins

The cDNAs coding for human AURKA (UniProt ID: O14965) and human CEP192 (UniProt ID: Q8TEP8) were synthesized by IDT (Integrated DNA Technologies, Coralville, IA) as gBlocks. All the

primers used in cloning are listed in table S2. Human AURKA$_{123–403}$ was cloned between the Nde I and Bam HI sites of vector pET15b (NEB, Ipswich, MA), and human CEP192$_{456–631}$, CEP192$_{456–541}$, CEP192$_{491–541}$, CEP192$_{506–536}$, CEP192$_{506–530}$, CEP192$_{506–527}$, CEP192$_{506–524}$, and CEP192$_{509–527}$ were cloned between the Bam HI and Sal I sites of vector pMAL-c2x (NEB). Point mutations were introduced using a method described previously (*66*). CEP192-AURKA$_{chimera}$ was cloned into pET15b, and CEP192$_{1–995}$ was cloned into modified pFastbac1, which adds a His$_6$-tag at the N terminus of the target protein, using a Gibson assembly method (*69*). All the AURKA proteins as well as CEP192-AURKA$_{chimera}$ were expressed in *Escherichia coli* BL21 (DE3) cells (Invitrogen, Carlsbad, CA), grown in Terrific Broth medium at 37°C until the OD$_{600}$ (optical density at 600 nm) reached a value of 1.5 to 2, followed by 16 hours at 19°C in the presence of 0.25 mM isopropyl-β-D-thiogalactoside. The cells were collected by centrifugation, resuspended in 50 mM tris (pH 8.0), 500 mM NaCl, 4 mM benzamidine hydrochloride, and 1 mM tris (2-carboxyethyl) phosphine (TCEP) (buffer A), and lysed using a ultrasonication. The proteins were loaded on a Ni–nitrilotriacetic acid (NTA) affinity column equilibrated with buffer A. The proteins were eluted with buffer A, supplemented with 300 mM imidazole. The His$_6$-tag of CEP192-AURKA$_{chimera}$ was removed by incubation with tobacco etch virus (TEV) protease overnight at 4°C. The proteins were additionally purified by gel filtration on a SD200HL 26/60 column (GE HealthCare, Chicago, IL) in 20 mM tris (pH 7.0), 100 mM NaCl, and 1 mM TCEP (buffer B). For kinase assays, purified AURKA constructs were concentrated to ~25 μM, aliquoted, and stored at −80°C.

To obtain dephosphorylated AURKA$_{123–403}$C290,393A, the protein was coexpressed with untagged lambda phosphatase cloned in pET cotransformation vector (13S-A), which was a gift from J. Chodera, N. Levinson, and M. Seeliger (Addgene plasmid #79748) (*70*). AURKA$_{123–403}$C290,393A coexpressed with lambda phosphatase was purified on a Ni-NTA affinity columnequilibrated with buffer A. The protein was eluted with buffer A, supplemented with 300 mM imidazole. In addition, 4000 U of lambda phosphatase (NEB) and 2 mM $MnCl_2$ were introduced to the eluted protein and incubated at room temperature (RT) for 1 hour, to fully dephosphorylate the protein, and the reaction was stopped by addition of 1 mM sodium orthovanadate (Sigma-Aldrich), as previously described (*71*). The protein was dialyzed onto a low-salt buffer [20 mM tris (pH 7.0), 100 mM NaCl, and 1 mM TCEP], loaded onto a cation exchange HiPrep SP HP 16/10 column (GE HealthCare), and eluted with a gradient from 0 to 100% high-salt buffer [20 mM tris (pH 7.0), 1 M NaCl, and 1 mM TCEP]. For kinase assays, purified dephosphorylated AURKA$_{123–403}$C290,393A was concentrated to ~25 μM, aliquoted, and stored at −80°C. The phosphorylation state of purified AURKA$_{123–403}$WT, AURKA$_{123–403}$ C290,393A, and dephosphorylated AURKA$_{123–403}$C290,393A was verified with liquid chromatography–electrospray ionization–mass spectrometry (LC-ESI-MS) and Western blot using anti-pT288 AURKA antibody (fig. S3).

All CEP192 proteins were expressed as described above except CEP192$_{1–995}$, which was expressed in *Spodoptera frugiperda* 9 cells (Expression Systems, Davis, CA) using the Bac-to-Bac baculovirus expression system according to the manufacturer's protocol (Invitrogen). For the purification of bacterially expressed CEP192 constructs, the cells were collected by centrifugation, resuspended in 20 mM tris (pH 7.5), 100 mM NaCl, 4 mM benzamidine hydrochloride, and 1 mM TCEP, and lysed using ultrasonication. The proteins were purified through an amylose affinity column according to the manufacturer's protocol (NEB). All the proteins were purified by gel filtration on an SD200HL 26/60 column (GE HealthCare) in buffer B.

*Sf*9-expressed CEP192$_{1–995}$ was purified on a Ni-NTA affinity column equilibrated with buffer A. The protein was eluted with buffer A, supplemented with 200 mM imidazole. The protein was additionally purified by gel filtration on a Superose 6 column (GE HealthCare, Chicago, IL) equilibrated in buffer B.

CEP192$_{506–536}$ (FITC-labeled and nonlabeled) and TPX2$_{1–43}$ (FITC-labeled and nonlabeled) peptides were synthesized by Anygen (Gwangju, South Korea). The peptides were subjected to three cycles of solubilization/lyophilization in 50% (v/v) methanol to remove any trifluoroacetic acid and acetonitrile remaining after reverse-phase purification and were reconstituted in appropriate buffer for downstream experiments.

Isothermal titration calorimetry

ITC measurements were carried out on a MicroCal iTC200 instrument (Malvern Panalytical, Worcestershire, UK). Protein samples were dialyzed for overnight at 4°C against 20 mM Hepes (pH 7.5), 100 mM NaCl, and 0.5 mM TCEP (ITC buffer). The CEP192$_{506–536}$ peptides were subjected to three cycles of solubilization/lyophilization in 50% (v/v) methanol to remove any trifluoroacetic acid and acetonitrile remaining that remained after reverse-phase purification, followed by a final solubilization in ITC buffer. The proteins (or the peptides) in the syringe were titrated at a concentration ~10-fold higher than that of the proteins in the ITC cell with a total volume of 200 μl, as indicated in the figures. Titrations consisted of 1-μl injections (lasting for 2 s) with an interval of 100 to 200 s between injections at 25°C. The heat of binding was corrected for the heat of injection, which was determined by injecting proteins into buffer. Data were analyzed using the program Origin (OriginLab, Northampton, MA). The parameters of the fit (stoichiometry and affinity) of each experiment are given in the figures.

Mass spectrometry

LC-ESI-MS analysis was performed using a Vanquish UHPLC system (Thermo Fisher Scientific, Waltham, MA) coupled to a Q Exactive Plus mass spectrometer (Thermo Fisher Scientific). Protein samples were separated on a BioResolve RP mAb Polyphenyl column (2.1 × 100 mm × 2.7 μm, 450 Å; Waters, Worcester, MA). The mobile phase consisted of buffer A: H_2O/formic acid (FA) = 100/0.1 (v/v) and buffer B: acetonitrile/FA = 100/0.1 (v/v). MS analysis was performed using in-source collision-induced dissociation with a collision energy of 30.0 eV. The scan type was full MS with simultaneous fragmentation and five microscans per spectrum. The maximum injection time was set to 150 ms, and the scan range was 500 to 6000 mass-to-charge ratio (m/z). Data were processed and analyzed using Xcalibur software (Thermo Fisher Scientific). The intact mass of the proteins was determined by deconvolution of the mass spectrum using the maximum entropy algorithm.

Multiangle light scattering

Samples were separated by size exclusion chromatography on a Superose 6 Increase 10/300 GL column (GE HealthCare)

equilibrated with 20 mM tris (pH 7.5), 100 mM NaCl, and 1 mM dithiothreitol (DTT). Multiangle light scattering was measured in line using a DAWN-HELEOS Multiangle light scattering detector and an Optilab rEX refractive index detector. The scattering data were analyzed with the ASTRA software (Wyatt Technology, Santa Barbara, CA).

Fluorescence polarization

A dilution series of $AURKA_{123–403}$ proteins was mixed with 50 nM FITC-labeled $CEP192_{506–536}$ or FITC-labeled $TPX2_{1–43}$ peptides in a reaction buffer containing 20 mM tris (pH 7.5), 100 mM NaCl, 1 mM DTT, and 1 mM $MgCl_2$. The reaction mixture in a 384-well plate (Corning, Corning, NY, #3575) was incubated at 25°C for 30 min, and the FP signal was measured with an EnVision microplate reader (PerkinElmer, Waltham, MA) by using 480- and 535-nm filters (for excitation and emission, respectively). The FP signal was analyzed with Prism 9 (GraphPad, San Diego, CA) using the equation $\Delta FP = FP - FPfree = (\Delta FPmax\ [protein])/(K_d + [protein])$, where FPfree is the background polarization signal (no protein, measured), ΔFPmax is the maximum polarization change (calculated), [protein] is the protein concentration, and K_d is the dissociation constant. Each experiment was performed in triplicate.

In competitive FP measurements, 1 μM $AURKA_{123–403}$ (the concentration of which achieves ~50% of complex formation based on the direct titration measurement) in the same reaction buffer was premixed with 50 nM FITC-labeled $CEP192_{506–536}$ or FITC-labeled $TPX2_{1–43}$ peptides. A dilution series of the nonlabeled peptides was then mixed with $AURKA_{123–403}$-FITC–labeled peptide mixture, and the FP measurement was carried out identically as described above. The FP signal was analyzed with Prism 9 (GraphPad), using the equation $\Delta FP = \Delta FP_0 - \Delta FPmax/1 + 10 \cdot e([peptide] - IC_{50})$, where ΔFP_0 is the polarization change without nonlabeled peptide, ΔFPmax is the maximum polarization change (calculated), [peptide] is the nonlabeled peptide concentration, and IC_{50} is the half-maximal inhibitory concentration. Each experiment was performed in triplicate.

ADP-Glo kinase assay

The kinase activity of AURKA was measured using the ADP-Glo kinase assay kit (Promega, Madison, WI). Purified phosphorylated $AURKA_{123–403}$WT, phosphorylated $AURKA_{123–403}$C290,393A, and dephosphorylated $AURKA_{123–403}$C290,393A stored at −80°C (25 μM stock solution) were defrosted at RT and diluted to the appropriate concentrations in the kinase assay buffer [20 mM tris-HCl (pH 7.5), 100 mM NaCl, 20 mM $MgCl_2$, 1 mM DTT, and bovine serum albumin (BSA) (0.1 mg ml^{-1})]. The diluted proteins were then mixed with appropriate concentrations of $TPX2_{1–43}$, $CEP192_{506–536}$, or $CEP192_{1–995}$ (stock concentration: 25 μM) to a total volume of 10 μl. The kinase reaction was initiated by adding mixture of ATP (Promega, from 10 mM stock solution to a final concentration of 50 μM) and the myelin basic protein–derived peptide substrate (sequence: VHFFKNIVTPRTP) (Tocris, Bristol, UK, to a final concentration of 0.2 mg ml^{-1}), to a total volume of 15 μl in 384-well plates (Corning, #3825). The reaction mixture was incubated at RT for 1 hour, at which time 5 μl of ADP-Glo reagent was added to stop the reaction and deplete the remaining ATP. After 1 hour of incubation at RT, 10 μl of kinase detection reagent was added to each well and incubated for 30 min. ATP consumption was measured on the basis of the luminescence generated from each well. The luminescence measured in the absence of ATP was subtracted as a background signal. The data were fitted to a three-parameter dose response model using the nonlinear regression function in Prism 9 (GraphPad). Each experiment was performed in triplicate.

Western blotting

Purified dephosphorylated $AURKA_{123–403}$C290,393A stored at −80°C (25 μM stock solution) was defrosted at RT and diluted to the appropriate concentrations in the kinase assay buffer [20 mM tris-HCl (pH 7.5), 100 mM NaCl, 20 mM $MgCl_2$, 1 mM DTT, and BSA (0.1 mg ml^{-1})]. The diluted proteins were then mixed with appropriate concentrations of $TPX2_{1–43}$, $CEP192_{506–536}$, or $CEP192_{1–995}$ (stock concentration: 25 μM) to a total volume of 9 μl. The kinase reaction was initiated by adding ATP (Promega; from 10 mM stock solution to a final concentration of 1 mM) to a total volume of 10 μl. After incubation at RT for 10 min, reactions were stopped by adding 2% SDS. The reactants were run on a 12% SDS–polyacrylamide gel electrophoresis gel and electrophoretically transferred onto a nitrocellulose membrane. The membrane was blocked for 30 min at RT with blocking buffer (tris-buffered saline containing 0.1% Tween 20 and 5% skim milk). The membranes were then probed with the indicated primary antibodies (anti–phospho-Thr^{288} AURKA, Cell Signaling Technology, #3079, 1:20,000; anti-AURKA, Invitrogen, #MA4-58900-A647, 1:10,000) and horseradish peroxidase–conjugated secondary antibodies (goat anti-rabbit, Abcam, #ab97051, 1:10,000; goat anti-mouse, Santa Cruz Biotechnology, #sc-5612, 1:10,000).

Crystallization and structure determination

Purified CEP192-$AURKA_{chimera}$ at ~15 mg ml^{-1} in 20 mM tris (pH 7.5), 100 mM NaCl, 1 mM DTT, 1 mM $MgCl_2$, and 1 mM ADP was used for the initial screening of crystallization conditions. Crystals were obtained at 16°C using the hanging-drop vapor diffusion method. The crystallization drop consisted of a 1:1 (v/v) mixture of protein solution and well solution containing 0.1 M tris (pH 8.0), 0.2 M lithium sulfate, and 15% (w/v) polyethylene glycol 3350. The quality of the crystals was further improved by microseeding. The crystals were flash-frozen in liquid nitrogen using a cryo-solution consisting of crystallization buffer supplemented with 30 to 35% (v/v) glycerol. X-ray datasets were collected at the Pohang Accelerator Laboratory (PAL) beamline BL-5C. The diffraction datasets were processed using HKL2000 (*72*). The structure was solved by molecular replacement using Phaser (*73*) with the kinase domain of AURKA (PDB ID: 5DT3) as a search model. The initial molecular replacement solution was refined using the program Refmac5 (*74*) and manually rebuilt with the program COOT (*75*). The structure was further refined with the program PHENIX (*76*) and iterative model building with COOT. In the final stages of the refinement cycle with PHENIX, in which the fine adjustment of the bond angles, bond lengths, and torsion angles was performed, *xyz* refinement, real-space refinement, and individual *B*-factor refinement were used. Noncrystallographic symmetry (NCS) restraints/constraints were not applied during the course of refinement, as the implementation of NCS produced local artifacts in flexible regions and only resulted in a marginal drop in R_{free} value. Data collection and refinement statistics are listed in table S1. Structural figures were generated with the program PyMOL (Schrödinger, New York City, NY). Sequence alignments were generated with

the program MAFFT (*77*) and illustrated using either Jalview (*78*) or ESPript (*79*). The conservation scores of amino acids in sequence alignments were determined with the program Scorecons (*80*). Disorder prediction was calculated with the program IUPred2A (*81*).

Cell culture, transfection, and immunofluorescence

For transient transfection, human $CEP192_{506–530}$WT and $CEP192_{506–530}$F508S were cloned between the Pst I and Bam HI sites of the vector pEGFP-C1 (Takara Bio, Kusatsu, Japan). HeLa cells were cultured in Dulbecco's modified Eagle's medium (WelGENE, Daegu, Korea) supplemented with 10% fetal bovine serum (WelGENE).

For immunofluorescence microscopy, approximately 1×10^5 HeLa cells (human cervical carcinoma cell line; AmericanType Culture Collection, CCL-2) were seeded on each coverslipin a six-well plate. The next day, cells were transfected with appropriate plasmids (pEGFP-C1 empty vector, pEGFP-C1-GFP-$CEP192_{506–530}$WT, or pEGFP-C1-GFP-$CEP192_{506–530}$F508S) using Lipofectamine 3000 (Thermo Fisher Scientific) according to the manufacturer's instructions. Twenty-four hours after transfection, the cells were synchronized with nocodazole (100 ng ml^{-1}; Sigma-Aldrich) for 15 hours. The cells were then released by washing three times in phosphate-buffered saline (PBS) and incubated in fresh medium for 30 min. The cell cycle was confirmed by flow cytometry. The cells were fixed with ice-cold methanol, washed with PBS, and permeabilized for 30 min in PBS containing 0.1% Triton X-100 (Sigma-Aldrich). Cells were then blocked with 3% BSA for 30 min followed by staining with the indicated primary antibodies (anti-AURKA–Alexa 555, Abcam, #ab217712, 1:1000; anti-CEP192, Novus Biologicals, NBP1-28718, 1:500) and/or secondary antibody (goat anti-rabbit Alexa 647, 1:1000, Invitrogen, #A-21245) at RT for 1 hour or overnight at 4°C. After staining of DNA with Hoechst 33342 (Thermo Fisher Scientific) for 1 min, images were acquired using a confocal laser scanning microscope LSM800 with Airyscan (Carl Zeiss, Oberkochen, Germany). The images were analyzed using ImageJ (*82*).

Supplementary Materials

This PDF file includes:

Figs. S1 to S10
Tables S1 and S2

View/request a protocol for this paper from *Bio-protocol*.

REFERENCES AND NOTES

1. T. Marumoto, D. Zhang, H. Saya, Aurora-A—A guardian of poles. *Nat. Rev. Cancer* **5**, 42–50 (2005).
2. M. Carmena, W. C. Earnshaw, The cellular geography of aurora kinases. *Nat. Rev. Mol. Cell Biol.* **4**, 842–854 (2003).
3. V. Joukov, A. De Nicolo, Aurora-PLK1 cascades as key signaling modules in the regulation of mitosis. *Sci. Signal.* **11**, eaar4195 (2018).
4. N. Tavernier, F. Sicheri, L. Pintard, Aurora A kinase activation: Different means to different ends. *J. Cell Biol.* **220**, e202106128 (2021).
5. P. A. Eyers, E. Erikson, L. G. Chen, J. L. Maller, A novel mechanism for activation of the protein kinase Aurora A. *Curr. Biol.* **13**, 691–697 (2003).
6. V. Joukov, A. De Nicolo, A. Rodriguez, J. C. Walter, D. M. Livingston, Centrosomal protein of 192 kDa (Cep192) promotes centrosome-driven spindle assembly by engaging in organelle-specific Aurora A activation. *Proc. Natl. Acad. Sci. U.S.A.* **107**, 21022–21027 (2010).
7. V. Joukov, J. C. Walter, A. De Nicolo, The Cep192-organized aurora A-Plk1 cascade is essential for centrosome cycle and bipolar spindle assembly. *Mol. Cell* **55**, 578–591 (2014).
8. T. Hirota, N. Kunitoku, T. Sasayama, T. Marumoto, D. Zhang, M. Nitta, K. Hatakeyama, H. Saya, Aurora-A and an interacting activator, the LIM protein Ajuba, are required for mitotic commitment in human cells. *Cell* **114**, 585–598 (2003).
9. S. L. Prosser, L. Pelletier, Mitotic spindle assembly in animal cells: A fine balancing act. *Nat. Rev. Mol. Cell Biol.* **18**, 187–201 (2017).
10. A. S. Nikonova, I. Astsaturov, I. G. Serebriiskii, R. L. Dunbrack, E. A. Golemis, Aurora A kinase (AURKA) in normal and pathological cell division. *Cell. Mol. Life Sci.* **70**, 661–687 (2013).
11. M. A. Gomez-Ferreria, U. Rath, D. W. Buster, S. K. Chanda, J. S. Caldwell, D. R. Rines, D. J. Sharp, Human Cep192 is required for mitotic centrosome and spindle assembly. *Curr. Biol.* **17**, 1960–1966 (2007).
12. N. M. Levinson, The multifaceted allosteric regulation of Aurora kinase A. *Biochem. J.* **475**, 2025–2042 (2018).
13. A. Zorba, V. Buosi, S. Kutter, N. Kern, F. Pontiggia, Y. J. Cho, D. Kern, Molecular mechanism of Aurora A kinase autophosphorylation and its allosteric activation by TPX2. *eLife* **3**, e02667 (2014).
14. R. Bayliss, T. Sardon, I. Vernos, E. Conti, Structural basis of Aurora-A activation by TPX2 at the mitotic spindle. *Mol. Cell* **12**, 851–862 (2003).
15. S. Cyphers, E. F. Ruff, J. M. Behr, J. D. Chodera, N. M. Levinson, A water-mediated allosteric network governs activation of Aurora kinase A. *Nat. Chem. Biol.* **13**, 402–408 (2017).
16. O. J. Gruss, R. E. Carazo-Salas, C. A. Schatz, G. Guarguaglini, J. Kast, M. Wilm, N. le Bot, I. Vernos, E. Karsenti, I. W. Mattaj, Ran induces spindle assembly by reversing the inhibitory effect of importin α on TPX2 activity. *Cell* **104**, 83–93 (2001).
17. T. Wittmann, M. Wilm, E. Karsenti, I. Vernos, TPX2, a novel xenopus MAP involved in spindle pole organization. *J. Cell Biol.* **149**, 1405–1418 (2000).
18. K. Zeng, R. N. Bastos, F. A. Barr, U. Gruneberg, Protein phosphatase 6 regulates mitotic spindle formation by controlling the T-loop phosphorylation state of Aurora A bound to its activator TPX2. *J. Cell Biol.* **191**, 1315–1332 (2010).
19. D. Hammond, K. Zeng, A. Espert, R. N. Bastos, R. D. Baron, U. Gruneberg, F. A. Barr, Melanoma-associated mutations in protein phosphatase 6 cause chromosome instability and DNA damage owing to dysregulated Aurora-A. *J. Cell Sci.* **126**, 3429–3440 (2013).
20. E. N. Pugacheva, E. A. Golemis, The focal adhesion scaffolding protein HEF1 regulates activation of the Aurora-A and Nek2 kinases at the centrosome. *Nat. Cell Biol.* **7**, 937–946 (2005).
21. D. Reboutier, M.-B. Troadec, J.-Y. Cremet, K. Fukasawa, C. Prigent, Nucleophosmin/B23 activates Aurora A at the centrosome through phosphorylation of serine 89. *J. Cell Biol.* **197**, 19–26 (2012).
22. C. P. Ponting, A novel domain suggests a ciliary function for ASPM, a brain size determining gene. *Bioinformatics* **22**, 1031–1035 (2006).
23. M. van Breugel, I. R. e Silva, A. Andreeva, Structural validation and assessment of AlphaFold2 predictions for centrosomal and centriolar proteins and their complexes. *Commun. Biol.* **5**, 312 (2022).
24. M. Mirdita, K. Schütze, Y. Moriwaki, L. Heo, S. Ovchinnikov, M. Steinegger, ColabFold: Making protein folding accessible to all. *Nat. Methods* **19**, 679–682 (2022).
25. J. Jumper, R. Evans, A. Pritzel, T. Green, M. Figurnov, O. Ronneberger, K. Tunyasuvunakool, R. Bates, A. Žídek, A. Potapenko, A. Bridgland, C. Meyer, S. A. A. Kohl, A. J. Ballard, A. Cowie, B. Romera-Paredes, S. Nikolov, R. Jain, J. Adler, T. Back, S. Petersen, D. Reiman, E. Clancy, M. Zielinski, M. Steinegger, M. Pacholska, T. Berghammer, S. Bodenstein, D. Silver, O. Vinyals, A. W. Senior, K. Kavukcuoglu, P. Kohli, D. Hassabis, Highly accurate protein structure prediction with AlphaFold. *Nature* **596**, 583–589 (2021).
26. Y. K. Rennie, P. J. McIntyre, T. Akindele, R. Bayliss, A. G. Jamieson, A TPX2 proteomimetic has enhanced affinity for Aurora-A due to hydrocarbon stapling of a helix. *ACS Chem. Biol.* **11**, 3383–3390 (2016).
27. E. F. Ruff, J. M. Muretta, A. R. Thompson, E. W. Lake, S. Cyphers, S. K. Albanese, S. M. Hanson, J. M. Behr, D. D. Thomas, J. D. Chodera, N. M. Levinson, A dynamic mechanism for allosteric activation of Aurora kinase A by activation loop phosphorylation. *eLife* **7**, e32766 (2018).
28. C. A. Dodson, R. Bayliss, Activation of Aurora-A kinase by protein partner binding and phosphorylation are independent and synergistic. *J. Biol. Chem.* **287**, 1150–1157 (2012).
29. K. Anderson, J. Yang, K. Koretke, K. Nurse, A. Calamari, R. B. Kirkpatrick, D. Patrick, D. Silva, P. J. Tummino, R. A. Copeland, Z. Lai, Binding of TPX2 to Aurora A alters substrate and inhibitor interactions. *Biochemistry* **46**, 10287–10295 (2007).
30. N. Tavernier, Y. Thomas, S. Vigneron, P. Maisonneuve, S. Orlicky, P. Mader, S. G. Regmi, L. van Hove, N. M. Levinson, G. Gasmi-Seabrook, N. Joly, M. Poteau, G. Velez-Aguilera, O. Gavet, A. Castro, M. Dasso, T. Lorca, F. Sicheri, L. Pintard, Bora phosphorylation substitutes in trans for T-loop phosphorylation in Aurora A to promote mitotic entry. *Nat. Commun.* **12**, 1899 (2021).
31. S. G. Burgess, R. Bayliss, The structure of C290A: C393A Aurora A provides structural insights into kinase regulation. *Acta Crystallogr. F* **71**, 315–319 (2015).

32. F. C. Rowan, M. Richards, R. A. Bibby, A. Thompson, R. Bayliss, J. Blagg, Insights into Aurora-A kinase activation using unnatural amino acids incorporated by chemical modification. *ACS Chem. Biol.* **8**, 2184–2191 (2013).
33. P. J. McIntyre, P. M. Collins, L. Vrzal, K. Birchall, L. H. Arnold, C. Mpamhanga, P. J. Coombs, S. G. Burgess, M. W. Richards, A. Winter, V. Veverka, F. von Delft, A. Merritt, R. Bayliss, Characterization of three druggable hot-spots in the Aurora-A/TPX2 interaction using biochemical, biophysical, and fragment-based approaches. *ACS Chem. Biol.* **12**, 2906–2914 (2017).
34. R. Bayliss, S. G. Burgess, P. J. McIntyre, Switching Aurora-A kinase on and off at an allosteric site. *FEBS J.* **284**, 2947–2954 (2017).
35. S. G. Burgess, M. Mukherjee, S. Sabir, N. Joseph, C. Gutiérrez-Caballero, M. W. Richards, N. Huguenin-Dezot, J. W. Chin, E. J. Kennedy, M. Pfuhl, S. J. Royle, F. Gergely, R. Bayliss, Mitotic spindle association of TACC3 requires Aurora-A-dependent stabilization of a cryptic α-helix. *EMBO J.* **37**, e97902 (2018).
36. E. H. Chan, A. Santamaria, H. H. Silljé, E. A. Nigg, Plk1 regulates mitotic Aurora A function through βTrCP-dependent degradation of hBora. *Chromosoma* **117**, 457–469 (2008).
37. C. Arter, L. Trask, S. Ward, S. Yeoh, R. Bayliss, Structural features of the protein kinase domain and targeted binding by small-molecule inhibitors. *J. Biol. Chem.* **298**, 102247 (2022).
38. E. W. Lake, J. M. Muretta, A. R. Thompson, D. M. Rasmussen, A. Majumdar, E. B. Faber, E. F. Ruff, D. D. Thomas, N. M. Levinson, Quantitative conformational profiling of kinase inhibitors reveals origins of selectivity for Aurora kinase activation states. *Proc. Natl. Acad. Sci. U.S.A.* **115**, E11894–E11903 (2018).
39. J. A. Gilburt, H. Sarkar, P. Sheldrake, J. Blagg, L. Ying, C. A. Dodson, Dynamic equilibrium of the aurora a kinase activation loop revealed by single-molecule spectroscopy. *Angew. Chem. Int. Ed. Engl.* **129**, 11567–11572 (2017).
40. I. W. Lee, Y. J. Jo, S. M. Jung, H. Y. Wang, N. H. Kim, S. Namgoong, Distinct roles of Cep192 and Cep152 in acentriolar MTOCs and spindle formation during mouse oocyte maturation. *FASEB J.* **32**, 625–638 (2018).
41. G. Vader, S. M. Lens, The Aurora kinase family in cell division and cancer. *Biochim. Biophys. Acta Rev. Cancer* **1786**, 60–72 (2008).
42. D. P. Byrne, S. Shrestha, M. Galler, M. Cao, L. A. Daly, A. E. Campbell, C. E. Eyers, E. A. Veal, N. Kannan, P. A. Eyers, Aurora A regulation by reversible cysteine oxidation reveals evolutionarily conserved redox control of Ser/Thr protein kinase activity. *Sci. Signal.* **13**, eaax2713 (2020).
43. D. C. Lim, V. Joukov, T. J. Rettenmaier, A. Kumagai, W. G. Dunphy, J. A. Wells, M. B. Yaffe, Redox priming promotes Aurora A activation during mitosis. *Sci. Signal.* **13**, eabb6707 (2020).
44. D. Karthigeyan, S. B. B. Prasad, J. Shandilya, S. Agrawal, T. K. Kundu, Biology of Aurora A kinase: Implications in cancer manifestation and therapy. *Med. Res. Rev.* **31**, 757–793 (2011).
45. Y. Tsuchiya, D. P. Byrne, S. G. Burgess, J. Bormann, J. Baković, Y. Huang, A. Zhyvoloup, B. Y. K. Yu, S. Peak-Chew, T. Tran, F. Bellany, A. B. Tabor, A. W. E. Chan, L. Guruprasad, O. Garifulin, V. Filonenko, M. Vonderach, S. Ferries, C. E. Eyers, J. Carroll, M. Skehel, R. Bayliss, P. A. Eyers, I. Gout, Covalent Aurora A regulation by the metabolic integrator coenzyme A. *Redox Biol.* **28**, 101318 (2020).
46. F. Sessa, M. Mapelli, C. Ciferri, C. Tarricone, L. B. Areces, T. R. Schneider, P. T. Stukenberg, A. Musacchio, Mechanism of Aurora B activation by INCENP and inhibition by hesperadin. *Mol. Cell* **18**, 379–391 (2005).
47. Z. Xu, H. Ogawa, P. Vagnarelli, J. H. Bergmann, D. F. Hudson, S. Ruchaud, T. Fukagawa, W. C. Earnshaw, K. Samejima, INCENP–Aurora B interactions modulate kinase activity and chromosome passenger complex localization. *J. Cell Biol.* **187**, 637–653 (2009).
48. R. Honda, R. Korner, E. A. Nigg, Exploring the functional interactions between Aurora B, INCENP, and survivin in mitosis. *Mol. Biol. Cell* **14**, 3325–3341 (2003).
49. M. Carmena, M. Wheelock, H. Funabiki, W. C. Earnshaw, The chromosomal passenger complex (CPC): From easy rider to the godfather of mitosis. *Nat. Rev. Mol. Cell Biol.* **13**, 789–803 (2012).
50. K. R. Abdul Azeez, S. Chatterjee, C. Yu, T. R. Golub, F. Sobott, J. M. Elkins, Structural mechanism of synergistic activation of Aurora kinase B/C by phosphorylated INCENP. *Nat. Commun.* **10**, 3166 (2019).
51. Y. Yasui, T. Urano, A. Kawajiri, K. I. Nagata, M. Tatsuka, H. Saya, K. Furukawa, T. Takahashi, I. Izawa, M. Inagaki, Autophosphorylation of a newly identified site of Aurora-B is indispensable for cytokinesis. *J. Biol. Chem.* **279**, 12997–13003 (2004).
52. K. B. Schou, S. K. Morthorst, S. T. Christensen, L. B. Pedersen, Identification of conserved, centrosome-targeting ASH domains in TRAPPII complex subunits and TRAPPC8. *Cilia* **3**, 1–12 (2014).
53. C. A. Kemp, K. R. Kopish, P. Zipperlen, J. Ahringer, K. F. O'Connell, Centrosome maturation and duplication in C. elegans require the coiled-coil protein SPD-2. *Dev. Cell* **6**, 511–523 (2004).
54. S. C. Moser, D. Bensaddek, B. Ortmann, J. F. Maure, S. Mudie, J. J. Blow, A. I. Lamond, J. R. Swedlow, S. Rocha, PHD1 links cell-cycle progression to oxygen sensing through hydroxylation of the centrosomal protein Cep192. *Dev. Cell* **26**, 381–392 (2013).
55. A. O. Walter, W. Seghezzi, W. Korver, J. Sheung, E. Lees, The mitotic serine/threonine kinase Aurora2/AIK is regulated by phosphorylation and degradation. *Oncogene* **19**, 4906–4916 (2000).
56. L. E. Littlepage, H. Wu, T. Andresson, J. K. Deanehan, L. T. Amundadottir, J. V. Ruderman, Identification of phosphorylated residues that affect the activity of the mitotic kinase Aurora-A. *Proc. Natl. Acad. Sci. U.S.A.* **99**, 15440–15445 (2002).
57. I. A. Asteriti, F. De Mattia, G. Guarguaglini, Cross-talk between AURKA and Plk1 in mitotic entry and spindle assembly. *Front. Oncol.* **5**, 283 (2015).
58. A. N. Kettenbach, K. A. Schlosser, S. P. Lyons, I. Nasa, J. Gui, M. E. Adamo, S. A. Gerber, Global assessment of its network dynamics reveals that the kinase Plk1 inhibits the phosphatase PP6 to promote Aurora A activity. *Sci. Signal.* **11**, eaaq1441 (2018).
59. A. Seki, J. A. Coppinger, C.-Y. Jang, J. R. Yates, G. Fang, Bora and the kinase Aurora a cooperatively activate the kinase Plk1 and control mitotic entry. *Science* **320**, 1655–1658 (2008).
60. L. Macůrek, A. Lindqvist, D. Lim, M. A. Lampson, R. Klompmaker, R. Freire, C. Clouin, S. S. Taylor, M. B. Yaffe, R. H. Medema, Polo-like kinase-1 is activated by aurora A to promote checkpoint recovery. *Nature* **455**, 119–123 (2008).
61. W. Bruinsma, M. Aprelia, J. Kool, L. Macurek, A. Lindqvist, R. H. Medema, Spatial separation of Plk1 phosphorylation and activity. *Front. Oncol.* **5**, 132 (2015).
62. N. Keen, S. Taylor, Aurora-kinase inhibitors as anticancer agents. *Nat. Rev. Cancer* **4**, 927–936 (2004).
63. B. Adhikari, J. Bozilovic, M. Diebold, J. D. Schwarz, J. Hofstetter, M. Schröder, M. Wanior, A. Narain, M. Vogt, N. Dudvarski Stankovic, A. Baluapuri, L. Schönemann, L. Eing, P. Bhandare, B. Kuster, A. Schlosser, S. Heinzlmeir, C. Sotriffer, S. Knapp, E. Wolf, PROTAC-mediated degradation reveals a non-catalytic function of AURORA-A kinase. *Nat. Chem. Biol.* **16**, 1179–1188 (2020).
64. E. Guarino Almeida, X. Renaudin, A. R. Venkitaraman, A kinase-independent function for AURORA-A in replisome assembly during DNA replication initiation. *Nucleic Acids Res.* **48**, 7844–7855 (2020).
65. Z. Wang, W. Huang, K. Zhou, X. Ren, K. Ding, Targeting the non-catalytic functions: A new paradigm for kinase drug discovery? *J. Med. Chem.* **65**, 1735–1748 (2022).
66. D. J. Cole, M. Janecek, J. E. Stokes, M. Rossmann, J. C. Faver, G. J. McKenzie, A. R. Venkitaraman, M. Hyvönen, D. R. Spring, D. J. Huggins, W. L. Jorgensen, Computationally-guided optimization of small-molecule inhibitors of the Aurora A kinase–TPX2 protein–Protein interaction. *Chem. Commun.* **53**, 9372–9375 (2017).
67. M. Janeček, M. Rossmann, P. Sharma, A. Emery, D. J. Huggins, S. R. Stockwell, J. E. Stokes, Y. S. Tan, E. G. Almeida, B. Hardwick, A. J. Narvaez, M. Hyvönen, D. R. Spring, G. J. McKenzie, A. R. Venkitaraman, Allosteric modulation of AURKA kinase activity by a small-molecule inhibitor of its protein-protein interaction with TPX2. *Sci. Rep.* **6**, 28528 (2016).
68. A. Zorba, V. Nguyen, A. Koide, M. Hoemberger, Y. Zheng, S. Kutter, C. Kim, S. Koide, D. Kern, Allosteric modulation of a human protein kinase with monobodies. *Proc. Natl. Acad. Sci. U.S.A.* **116**, 13937–13942 (2019).
69. D. G. Gibson, L. Young, R. Y. Chuang, J. C. Venter, C. A. Hutchison III, H. O. Smith, Enzymatic assembly of DNA molecules up to several hundred kilobases. *Nat. Methods* **6**, 343–345 (2009).
70. S. K. Albanese, D. L. Parton, M. Işık, L. Rodríguez-Laureano, S. M. Hanson, J. M. Behr, S. Gradia, C. Jeans, N. M. Levinson, M. A. Seeliger, J. D. Chodera, An open library of human kinase domain constructs for automated bacterial expression. *Biochemistry* **57**, 4675–4689 (2018).
71. D. L. Satinover, C. A. Leach, P. T. Stukenberg, D. L. Brautigan, Activation of Aurora-A kinase by protein phosphatase inhibitor-2, a bifunctional signaling protein. *Proc. Natl. Acad. Sci. U.S.A.* **101**, 8625–8630 (2004).
72. Z. Otwinowski, W. Minor, Processing of X-ray diffraction data collected in oscillation mode. *Methods Enzymol.* **276**, 307–326 (1997).
73. A. J. McCoy, R. W. Grosse-Kunstleve, P. D. Adams, M. D. Winn, L. C. Storoni, R. J. Read, Phaser crystallographic software. *J. Appl. Cryst.* **40**, 658–674 (2007).
74. G. N. Murshudov, P. Skubák, A. A. Lebedev, N. S. Pannu, R. A. Steiner, R. A. Nicholls, M. D. Winn, F. Long, A. A. Vagin, REFMAC5 for the refinement of macromolecular crystal structures. *Acta Crystallogr. D* **67**, 355–367 (2011).
75. P. Emsley, B. Lohkamp, W. G. Scott, K. Cowtan, Features and development of Coot. *Acta Crystallogr. D* **66**, 486–501 (2010).
76. D. Liebschner, P. V. Afonine, M. L. Baker, G. Bunkóczi, V. B. Chen, T. I. Croll, B. Hintze, L. W. Hung, S. Jain, A. J. McCoy, N. W. Moriarty, R. D. Oeffner, B. K. Poon, M. G. Prisant, R. J. Read, J. S. Richardson, D. C. Richardson, M. D. Sammito, O. V. Sobolev, D. H. Stockwell, T. C. Terwilliger, A. G. Urzhumtsev, L. L. Videau, C. J. Williams, P. D. Adams, Macromolecular

structure determination using X-rays, neutrons and electrons: Recent developments in Phenix. *Acta Crystallogr. D* **75**, 861–877 (2019).
77. J. Rozewicki, S. Li, K. M. Amada, D. M. Standley, K. Katoh, MAFFT-DASH: Integrated protein sequence and structural alignment. *Nucleic Acids Res.* **47**, W5–W10 (2019).
78. A. M. Waterhouse, J. B. Procter, D. M. Martin, M. Clamp, G. J. Barton, Jalview Version 2—A multiple sequence alignment editor and analysis workbench. *Bioinformatics* **25**, 1189–1191 (2009).
79. P. Gouet, X. Robert, E. Courcelle, ESPript/ENDscript: Extracting and rendering sequence and 3D information from atomic structures of proteins. *Nucleic Acids Res.* **31**, 3320–3323 (2003).
80. W. S. Valdar, Scoring residue conservation. *Proteins* **48**, 227–241 (2002).
81. B. Mészáros, G. Erdős, Z. Dosztányi, IUPred2A: Context-dependent prediction of protein disorder as a function of redox state and protein binding. *Nucleic Acids Res.* **46**, W329–W337 (2018).
82. M. D. Abràmoff, P. J. Magalhães, S. J. Ram, Image processing with ImageJ. *Biophotonics Int.* **11**, 36–42 (2004).

Acknowledgments: We thank Hak Suk Chung for help with x-ray diffraction data collection and analysis. We also thank beamline staff at the Pohang Accelerator Laboratory (Beamline BL-5C, BL-7A, and BL-11C) for assistance with the x-ray diffraction experiments. **Funding:** This work was supported by the research support program of the Lim Sung Ki Foundation (LF-RSP2022-02), by the intramural grants of Korea Institute of Science and Technology (KIST, no. 2E32333 and 2V09702), and by the National research council of Science and Technology (NST) grant from the Korean government (MSIT, no. CPS21061-100). **Author contributions:** I.-G.L. conceived and led the study. J.-G.P. and I.-G.L. designed and performed the biochemical, structural, and cellular experiments. H.J. purified the proteins. S.S. collected and analyzed the x-ray diffraction data. C.S. and H.L. performed the cellular experiments and provided technical expertise. K.Y.H., E.E.K., and B.-J.L. curated and analyzed the data. N.-K.K. performed multiangle light scattering. J.-G.P. and I.-G.L. wrote the manuscript. **Competing interests:** The authors declare that they have no competing interests. **Data and materials availability:** Atomic coordinates and structure factors for the structure of CEP192-AURKA$_{chimera}$ were deposited with the Protein Data Bank (PDB) under accession code 8GUW. All data needed to evaluate the conclusions in the paper are present in the paper and/or the Supplementary Materials.

Submitted 17 November 2022
Accepted 17 March 2023
Published 21 April 2023
10.1126/sciadv.adf8582